6-Methyl-6-(*p*-chlorophenyl)fulvene was obtained as a viscous, dark orange liquid in 56% yield from 0.084 mol of *p*-chloroacetophenone. MS, *m/e* 207, 205 (M^+, $C_{13}H_{11}Cl$).

6-Methyl-6-(*p*-bromophenyl)fulvene. Reaction of *p*-bromoacetophenone (0.084 mol) with cyclopentadiene afforded a 68% yield of 6-methyl-6-(*p*-bromophenyl)fulvene as a dark orange, viscous oil. MS, *m/e* 246 (M^+, ^{79}Br), 248 (M^+, ^{81}Br), 233 and 231 ($M^+ - CH_3$), 167 ($M^+ - Br$).

6-Methyl-6-(*p*-acetylphenyl)fulvene was prepared by reaction of *p*-diacetylbenzene (0.074 mol) with 1 equiv of monomeric cyclopentadiene, as described above, for 45 min. Chromatography (silica gel; CH_2Cl_2 eluant) afforded 3.1 g (20%) of product as an orange powder, mp 90.0–91.5 °C. Anal. Calcd for $C_{15}H_{14}O$: C, 85.67; H, 6.71. Found: C, 85.07; H, 6.99. MS, *m/e* 210 (M^+), 195 ($M - CH_3$), 167 ($M - CH_3CO$).

6-Methyl-6-(*p*-cyanophenyl)fulvene. Reaction of 0.069 mol of *p*-cyanoacetophenone with an equimolar amount of cyclopentadiene for 1.5 h gave 6-methyl-6-(*p*-cyanophenyl)fulvene as an orange oil in 36% yield. MS, *m/e* 193 (M^+), 178 ($M - CH_3$).

Acknowledgment. We gratefully acknowledge the technical assistance of Doris LaSpina and Fred Carter in the early stages of this work, and of Professor George Vogel, who ran the mass spectra for us.

Registry No. 6-Methyl-6-phenylfulvene, 2320-32-3; 6-methyl-6-(*p*-aminophenyl)fulvene, 91158-21-3; 6-methyl-6-(*p*-tolyl)fulvene, 38069-02-2; 6-methyl-6-(*p*-chlorophenyl)fulvene, 13347-54-1; 6-methyl-6-(*p*-anisyl)fulvene, 38069-03-3; 6-methyl-6-(*p*-fluorophenyl)fulvene, 78405-51-3; 6-methyl-6-(*p*-bromophenyl)fulvene, 32884-56-3; 6-methyl-6-(*p*-acetylphenyl)fulvene, 91158-22-4; 6-methyl-6-(*p*-cyanophenyl)fulvene, 91158-23-5; 6-(*p*-aminophenyl)fulvene, 91158-24-6; 6-(*p*-hydroxyphenyl)fulvene, 91158-25-7; 6-(*p*-tolyl)fulvene, 32884-55-2; 6-phenylfulvene, 7338-50-3; 6-(*p*-chlorophenyl)fulvene, 32884-54-1; cyclopentadiene, 542-92-7; *p*-aminoacetophenone, 99-92-3; *p*-methoxyacetophenone, 100-06-1; *p*-methylacetophenone, 122-00-9; *p*-fluoroacetophenone, 403-42-9; *p*-chloroacetophenone, 99-91-2; *p*-bromoacetophenone, 99-90-1; *p*-diacetylbenzene, 1009-61-6; *p*-cyanoacetophenone, 1443-80-7.

Iron-Containing Metallophosphazenes and Their Clusters Derived from Chlorophosphazenes and Organometallic Dianions[1]

Harry R. Allcock,*† Paul R. Suszko,† Linda J. Wagner,† Robert R. Whittle,† and Brian Boso‡

Contribution from the Departments of Chemistry and Physics, The Pennsylvania State University, University Park, Pennsylvania 16802. *Received November 10, 1983*

Abstract: Hexachlorocyclotriphosphazene, $(NPCl_2)_3$, reacts with disodium octacarbonyldiferrate, $Na_2Fe_2(CO)_8$, to yield the diiron and triiron cyclotriphosphazene complexes **2** and **3**, respectively. The analogous cyclic tetramer $(NPCl_2)_4$ reacts similarly to yield the diiron and triiron analogues **5** and **6**, respectively. Compounds **2** and **5** are the first *chlorophosphazenes* that contain two metal–phosphorus covalent bonds and a three-membered spirocyclic ring at phosphorus. Compound **3** can also be obtained by the thermal reaction of **2** with the neutral carbonyl complexes $Fe(CO)_5$ and $Fe_2(CO)_9$. In addition, the thermal reaction of **2** with $Ru_3(CO)_{12}$ yields the mixed-metal cluster **7**, similar in structure to **3**, but with a $Ru(CO)_3$ unit in place of the nitrogen-bound $Fe(CO)_3$. The trimetallic clusters **3**, **6**, and **7** are the first phosphazene compounds in which a portion of the phosphazene ring has been incorporated into a metallic cluster unit. Compounds **3**, **6**, and **7** contain both phosphorus–metal and nitrogen–metal bonds, demonstrating both the covalent and coordinative capacities of phosphazene rings. The new metallophosphazenes were characterized by ^{31}P NMR, Mössbauer, infrared, and mass spectral techniques and by X-ray crystal structure analyses.

The synthesis and characterization of new metal cluster compounds, and especially mixed-metal clusters, have attracted wide attention.[2] These species are of interest as new catalysts or catalyst precursors and have been examined as models for catalytic metal surfaces.[3] Our interest in this area stems from the realization that cyclic phosphazenes are potentially versatile multifunctional "ligands" for the stabilization of transition-metal compounds. Although a few transition-metal-linked phosphazenes have already been reported, this area remains relatively unexploited.

Several of the known examples of transition-metal-bound phosphazenes are adducts in which the skeletal nitrogen atoms function as electron-rich donors, especially when electron-supplying alkylamino and alkyl substituent groups are present.[4-11] For example, platinum dichloride complexes have been prepared via coordinative bonding to the lone-pair electrons on the backbone nitrogen atoms in aminophosphazenes of formula $[NP(NHCH_3)_2]_n$, where $n = 4$ or 15000.[11]

A number of complexes have also been prepared by the attachment of transition metals to pendent donor groups linked to either cyclic or high polymeric phosphazenes. These include phosphino,[12-14] *nido*-carboranyl,[15] acetyleno,[16,17] and ferrocenyl side groups.[18,19] The interactions of metal carbonyl compounds

† Department of Chemistry.
‡ Department of Physics.

(1) A preliminary communication on this work has appeared: Suszko, P. R.; Whittle, R. R.; Allcock, H. R. *J. Chem. Soc., Chem. Commun.* **1982**, 649.
(2) Gladfelter, W. L.; Geoffroy, G. L. *Adv. Organomet. Chem.* **1980**, *18*, 207 and references cited therein.
(3) Muetterties, E. L. *Chem. Eng. News*, **1982**, Aug 30, p 28 and references cited therein.
(4) Moeller, T.; Kokalis, S. G. *J. Inorg. Nucl. Chem.* **1963**, *25*, 875.
(5) Searle, H. T.; Dyson, J.; Ranganathan, T. N.; Paddock, N. L. *J. Chem. Soc., Dalton Trans.* **1975**, 203.
(6) Lappert, M. F.; Srivastava, G. *J. Chem. Soc. A* **1966**, *210*.
(7) Marsh, W. C.; Paddock, N. L.; Stewart, C. J.; Trotter, J. *J. Chem. Soc. D* **1970**, 1190.
(8) Calhoun, H. P.; Paddock, N. L.; Wingfield, J. N. *Can. J. Chem.* **1975**, *53*, 1765.
(9) Ratz, R.; Kober, E.; Grundman, C.; Ottmann, G. *Inorg. Chem.* **1964**, *3*, 757.
(10) Jenkins, R. W.; Lanoux, S. *J. Inorg. Nucl. Chem.* **1970**, *32*, 2429.
(11) (a) Allcock, H. R.; Allen, R. W.; O'Brien, J. P. *J. Am. Chem. Soc.* **1977**, *99*, 3984. (b) Allen, R. W.; O'Brien, J. P.; Allcock, H. R. *Ibid.* **1977**, *99*, 3987.
(12) Evans, T. L.; Fuller, T. J.; Allcock, H. R. *J. Am. Chem. Soc.* **1979**, *101*, 242.
(13) Allcock, H. R.; Fuller, T. J.; Evans, T. L. *Macromolecules* **1980**, *13*, 1325.

Scheme I

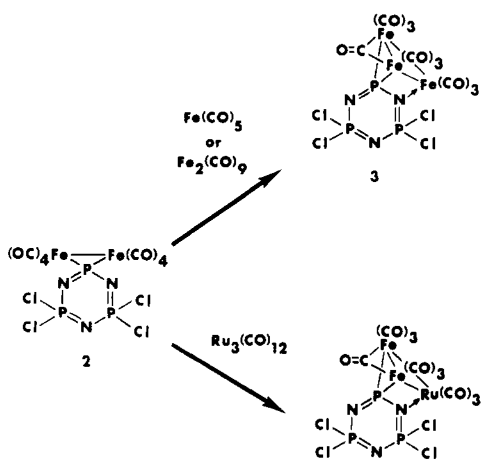

with cyclic phosphazenes is of special interest, and several amino-, alkyl-, and halogenophosphazenes have been reported to form molybdenum or tungsten coordination species.[20-23]

Recently, a new approach has been developed in our laboratory that leads to the preparation of phosphazenes with covalent phosphorus–metal bonds.[24-26] This approach involves the nucleophilic substitution reactions of organometallic anions with cyclic fluorophosphazenes. For example, the reactions of $M(CO)_2Cp^- K^+$ (M = Fe or Ru) with $(NPF_2)_3$ led to the sequential replacement of two geminal fluorine atoms by organometallic units, followed by decarbonylation and formation of a three-membered P–Fe–Fe spiro ring. However, so far it has proved difficult to extend these reactions to *chlorophosphazenes* because metal–halogen exchange apparently competes with nucleophilic substitution. This is a serious problem for the preparation of high polymeric metallophosphazenes because the high polymer $(NPCl_2)_n$ is much preferred over $(NPF_2)_n$ as a reaction substrate.

In this paper, we describe the use of organometallic dianions for metallocyclophosphazene synthesis. These reactions are suitable for use with *chlorophosphazene* substrates; hence, they are of considerable interest as prototypes for high polymer synthesis. It will be shown that these reactions lead to the formation of both spirometallophosphazenes and metallo cluster phosphazenes containing both single metal and mixed-metal units. Later sections of the paper contain ^{31}P NMR, infrared, Mössbauer, and X-ray diffraction evidence in favor of these structures.

Results and Discussion

The General Reaction. Hexachlorocyclotriphosphazene (**1**) reacts with disodium octacarbonyldiferrate in THF to yield a spiro diiron octacarbonyl bonded phosphazene (**2**) and a triiron deca-

(14) Allcock, H. R.; Lavin, K. D.; Tollefson, N. M.; Evans, T. L. *Organometallics* **1983**, *2*, 267.
(15) Allcock, H. R.; Scopelianos, A. G.; Whittle, R. R.; Tollefson, N. M. *J. Am. Chem. Soc.*, **1983**, *105*, 1316.
(16) Chivers, T. *Inorg. Nucl. Chem. Lett.* **1971**, *7*, 827.
(17) Allcock, H. R.; Harris, P. J.; Nissan, R. A. *J. Am. Chem. Soc.* **1981**, *103*, 2256 and unpublished results.
(18) Suszko, P. R.; Whittle, R. R.; Allcock, H. R. *J. Chem. Soc., Chem. Commun.* **1982**, 960.
(19) Allcock, H. R.; Lavin, K. D.; Riding, G. H.; Suszko, P. R.; Whittle, R. R. *J. Am. Chem. Soc.* **1984**, *106*, 2337.
(20) Dyson, J.; Paddock, N. L. *J. Chem. Soc., Chem. Commun.* **1966**, *7*, 191.
(21) Paddock, N. L.; Ranganathan, T. N.; Wingfield, J. N. *J. Chem. Soc., Dalton Trans.* **1972**, 1578.
(22) Cotton, F. A.; Rusholme, G. A.; Shaver, A. *J. Coord. Chem.* **1973**, *3*, 99.
(23) Hotas, N. K.; Harris, R. O. *J. Chem. Soc. D* **1972**, 407.
(24) Greigger, P. P.; Allcock, H. R. *J. Am. Chem. Soc.* **1979**, *101*, 2492.
(25) Allcock, H. R.; Greigger, P. P.; Wagner, L. J.; Bernheim, M. Y. *Inorg. Chem.* **1981**, *20*, 716.
(26) Allcock, H. R.; Wagner, L. J.; Levin, M. L. *J. Am. Chem. Soc.*, **1983**, *105*, 1321.

Table I. ^{31}P NMR[a] and Infrared[b] Spectroscopic Data

compound	IR, cm^{-1}		^{31}P NMR, δ
$N_3P_3Cl_4Fe_2(CO)_8$, **2**	2120 (m)	2039 (s)	A_2X pattern
	2076 (s)	2027 (s)	δ_A 13.1 (J_{AX} = 51)
	2051 (s)	2013 (w)	δ_X 222.5
$N_3P_3Cl_4Fe_3(CO)_{10}$, **3**	2093 (m)	2018 (m)	AMX pattern
	2057 (s)	2006 (m)	δ_A 14.5 (J_{AM} = 33)
	2044 (s)	1972 (br)	δ_M 27.1 (J_{AX} = 61)
	2030 (s)	1870 (br)	δ_X 217.9 (J_{MX} = 12)
$N_3P_3Cl_4Fe_2Ru(CO)_{10}$, **7**	2094 (m)	2004 (m)	AMX pattern
	2052 (s)	1995 (w, sh)	δ_A 13.6 (J_{AM} = 32)
	2023 (s)	1872 (br)	δ_M 24.6 (J_{AX} = 61)
			δ_X 226.3 (J_{MX} = 18)
$N_4P_4Cl_6Fe_2(CO)_8$, **5**	2120 (m)	2029 (s)	AM_2X pattern
	2076 (s)	2015 (w)	δ_A −5.3 (t, J_{AM} = 33)
	2051 (s)		δ_M −12.8 (dd, J_{MX} = 85)
	2041 (s)		δ_X 185.0 (t)
$N_4P_4Cl_6Fe_3(CO)_{10}$, **6**	2094 (m)	2016 (m)	AMRX pattern
	2057 (s)	2005 (m)	δ_A −11.3 (dd, J_{AM} = 19)
	2043 (s)	1972 (br)	δ_M −5.9 (dd, J_{AX} = 90)
	2030 (s)	1871 (br)	δ_R 2.5 (t, J_{MR} = 39)
			δ_X 183.8 (dd, J_{RX} = 41)

[a] All spectra are referenced to external H_3PO_4. In $CDCl_3$ solution. *J* values are given in hertz. [b] In hexane solution. In the carbonyl region.

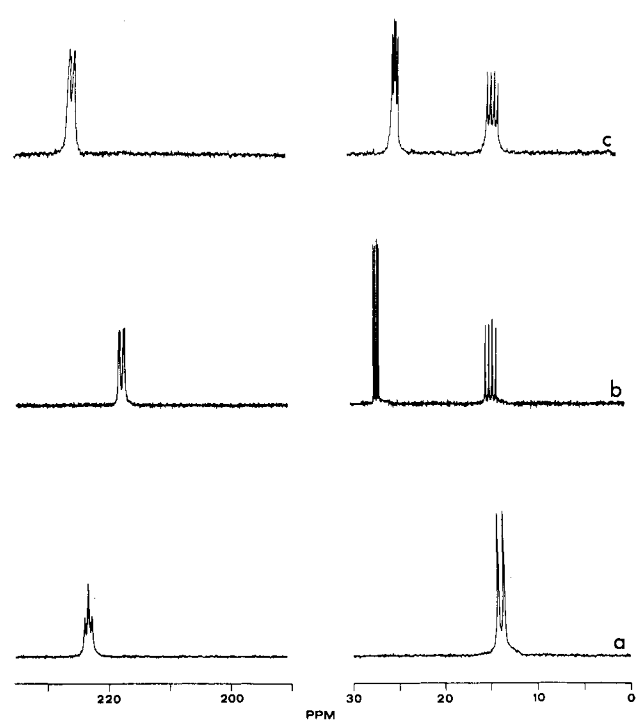

Figure 1. ^{31}P NMR spectra for **2** (spectrum a), **3** (spectrum b), and **7** (spectrum c).

Table II. Mössbauer Spectroscopic Data for Iron-Containing Metallophosphazenes[a]

	IS, mm/s	QS, mm/s	Γ, mm/s	% of tot area
$N_3P_3Cl_4Fe_2(CO)_8$, **2**	0.103	1.301	0.238	100
$N_3P_3Cl_4Fe_3(CO)_{10}$, **3**	0.263	0.508	0.240	31.2
	0.188	0.859	0.310	68.8
$N_3P_3Cl_4Fe_2Ru(CO)_{10}$, **7**	0.057	0.972	0.234	100
$N_4P_4Cl_6Fe_2(CO)_8$, **5**	−0.011	1.301	0.247	100
$N_4P_4Cl_6Fe_3(CO)_{10}$, **6**	0.229	0.600	0.230	27.9
	0.052	0.760	0.283	72.1

[a] IS = isomer shift; QS = quadrupole splitting; Γ = peak width at half height.

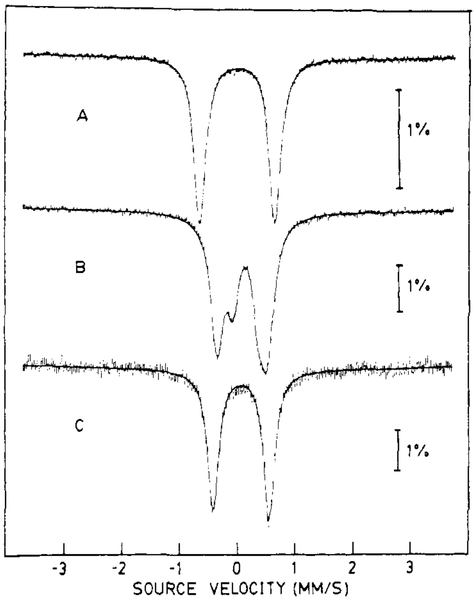

Figure 2. Mössbauer spectra for **2** (spectrum A), **3** (spectrum B), and **7** (spectrum C).

carbonyl bonded phosphazene (**3**). Similarly, octachlorocyclotetraphosphazene (**4**) reacts with the same reagent to form the analogous products **5** and **6**.

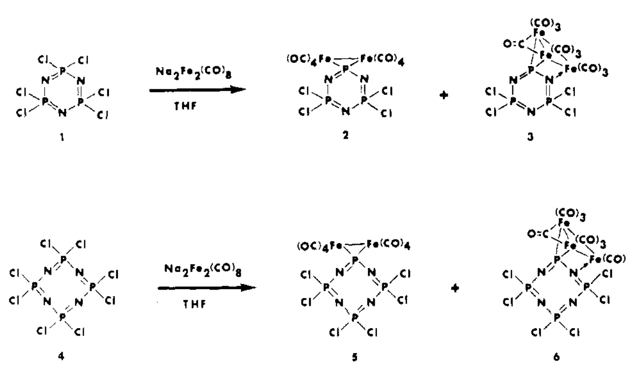

Compound **2** is an orange, crystalline material, which is stable in air for months with little evidence of decomposition. It is soluble in THF, chloroform, methylene chloride, and toluene and is moderately soluble in pentane or hexane. Solutions of **2** decompose slowly on exposure to air. The compound sublimes with partial decomposition at 60 °C (0.1 torr).

Species **3** was isolated in low yield (<2%) as a purple-black crystalline solid. This compound, too, is stable in air in the crystalline state and has similar sublimation characteristics to those of **2** and similar solubilities except for a greater solubility in aliphatic hydrocarbons. This compound is the first metallic cluster phosphazene. As discussed later, the structure of **3** is of interest because it contains both phosphorus–metal and nitrogen–metal bonds to the phosphazene ring.

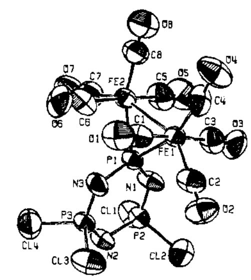

Figure 3. ORTEP diagram for compound **2**.

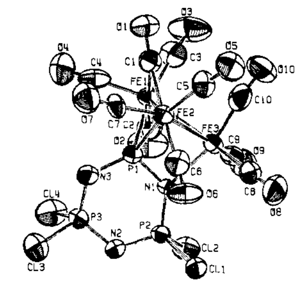

Figure 4. ORTEP diagram for compound **3**.

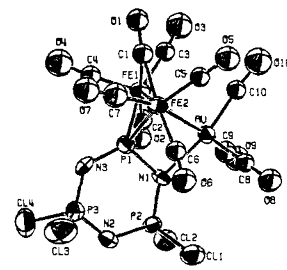

Figure 5. ORTEP diagram for compound **7**.

The physical properties of the tetrameric analogues are similar to those of the cyclic trimers (see Experimental Section).

Reaction Mechanisms. The preparation of $(CO)_4Fe^{-}$–$Fe^{-}(CO)_4$ has been discussed by Collman and co-workers.[27] Disodium tetracarbonylferrate reacts with iron pentacarbonyl to yield $Na_2Fe_2(CO)_8$ directly. It is also known that this latter reagent interacts with diphenylchlorophosphine to yield a diphosphido-bridged iron dimer[27] or with CH_2I_2 to give a methylene-bridged iron dimer.[28] Thus, the formation of **2** or **5** can be understood in terms of a sequential or near simultaneous geminal nucleophilic substitution by the dianion on **1** or **4**.

However, two questions are of special interest. (1) Why do the chlorophosphazenes $(NPCl_2)_{3\text{ and }4}$ react by this substitutive mechanism, whereas treatment of $(NPCl_2)_{3\text{ or }4}$ with $[Fe(CO)_2Cp]^-$ results in decomposition of the phosphazene? (2) What is the mechanism of formation of the cluster systems **3** and **6**?

The answer to the first question probably lies in the fact that $Na_2Fe_2(CO)_8$ is less reactive than is the $[FeCp(CO)_2]^-$ monoanionic reagent. It is, therefore, likely to follow a nucleophilic substitution pathway rather than a metal–halogen exchange route. A second contributing factor may be that, in $Na_2Fe_2(CO)_8$, the two negative charges are localized on the iron atoms and are ideally positioned for the displacement of two geminal chlorine atoms in **1** and **4**.

Clues to the mechanism of formation of the cluster metallophosphazenes are as follows. Compound **3** forms deep purple solutions in low concentrations. However, the mixture formed by the interaction of **1** with $Na_2Fe_2(CO)_8$ is maroon. Only after

(27) Collman, J. P.; Finke, R. G.; Matlock, P. L.; Wahren, R.; Brauman, J. I. *J. Am. Chem. Soc.* **1976**, *98*, 4685.
(28) Sumner, C. E., Jr.; Riley, P. E.; Davis, R. E.; Pettit, P. *J. Am. Chem. Soc.* **1980**, *102*, 1752.
(29) Wei, C. H.; Dahl, L. F. *J. Am. Chem. Soc.* **1969**, *91*, 1351.

Table III. Summary of Crystal Data and Intensity Collection Parameters

	2	3	7
fw, amu	612.53	747.44	792.61
space group	$P2_1$	$P4_2$	$P4_2$
a, Å	8.150 (3)	24.093 (5)	24.133 (4)
b, Å	16.723 (3)		
c, Å	15.556 (4)	8.580 (1)	8.574 (2)
α, deg			
β, deg	97.22 (3)		
γ, deg			
vol, Å^3	2103 (2)	4981 (3)	4994 (3)
Z	4	8	8
d(calcd), g/cm^3	1.934	1.992	2.047
cryst dimens, mm	0.31 × 0.25 × 0.30	0.26 × 0.29 × 0.38	0.15 × 0.15 × 0.33
A	0.67	1.0	0.75
bkgd	0.5	0.5	0.5
2θ limits, deg	3.0–45.28	3.0–46.0	3.4–46.0
data measd	3114	5784	5811
mean discrepancy of multipy measd reflcns		0.045	0.034
unique nonzero data	3106	3289	3604
obsd data ($I > 2\sigma(I)$)	3021	3083	3236
μ, cm^{-1}	18.40	24.30	24.04
R_1/R_2	0.059/0.064	0.056/0.060	0.051/0.056
goodness of fit	2.535	3.832	5.864
data/parameter	6.00	7.38	7.93
drift correction	0.927–1.044	0.979–1.097	0.933–1.017
recrystn solvent	hexane	toluene	toluene
largest residual peak,[a] e Å^{-3}	0.12	0.11	0.13

[a] Peak residuals are given relative to the intensity of a carbon atom (C = 6 e Å^{-3}).

Table IV. Bond Lengths (Å) for **2**

	A	B
Fe(1)–Fe(2)	2.742 (4)	2.750 (3)
Fe(1)–P(1)	2.263 (5)	2.218 (5)
Fe(2)–P(1)	2.238 (5)	2.184 (5)
Fe(1)–C(1)	1.83 (2)	1.83 (2)
Fe(1)–C(2)	1.76 (2)	1.74 (2)
Fe(1)–C(3)	1.86 (2)	1.81 (2)
Fe(1)–C(4)	1.71 (2)	1.88 (2)
Fe(2)–C(5)	1.84 (2)	1.88 (3)
Fe(2)–C(6)	1.80 (3)	1.80 (2)
Fe(2)–C(7)	1.92 (2)	1.81 (2)
Fe(2)–C(8)	1.79 (2)	1.86 (2)
P(2)–Cl(1)	1.974 (7)	2.002 (8)
P(2)–Cl(2)	2.001 (8)	2.006 (7)
P(3)–Cl(3)	2.002 (7)	1.998 (9)
P(3)–Cl(4)	1.985 (8)	1.989 (8)
P(1)–N(1)	1.63 (2)	1.62 (2)
P(1)–N(3)	1.64 (2)	1.64 (2)
P(2)–N(1)	1.52 (2)	1.55 (2)
P(3)–N(3)	1.53 (2)	1.55 (2)
P(2)–N(2)	1.64 (1)	1.55 (2)
P(3)–N(2)	1.58 (2)	1.59 (2)
C(1)–O(1)	1.10 (2)	1.10 (2)
C(2)–O(2)	1.17 (3)	1.14 (2)
C(3)–O(3)	1.11 (3)	1.11 (2)
C(4)–O(4)	1.20 (3)	1.11 (3)
C(5)–O(5)	1.11 (3)	1.06 (3)
C(6)–O(6)	1.13 (3)	1.13 (2)
C(7)–O(7)	1.06 (3)	1.14 (3)
C(8)–O(8)	1.14 (3)	1.15 (3)

removal of the reaction solvent and redissolution in hexane or methylene chloride does the characteristic color of **3** appear. ^{31}P NMR spectra obtained before removal of the reaction solvent were compatible with a complex mixture of **2** and other products, but **3** was not detected at this stage. Thus, **3** is probably formed from **2** during subsequent isolation.

The only air-stable products isolated (by column chromatography) were **2**, **3**, unreacted **1** (~80%), and $Fe_3(CO)_{12}$. It is presumed that this latter species is generated by oxidative coupling of iron carbonyl fragments during the isolation procedure. It is these fragments that are presumed to react with **2** or **5** to give **3** or **6**.

First, it was shown that **2** and **3** can be obtained in very low yield by the treatment of **1** with $Na_2Fe(CO)_4$ in THF. It is assumed that $Na_2Fe_2(CO)_8$ is formed in situ in this system and gives rise to **2**. $Fe(CO)_5$ was detected as another product, and this was believed to be resposible for the conversion of **2** to **3**.

In fact, treatment of a pure sample of **2** with either $Fe(CO)_5$ or $Fe_2(CO)_9$ in boiling hexane (Scheme I) yielded the cluster metallophosphazene **3** (Scheme I). With $Fe(CO)_5$, the formation of **3** is quite inefficient (<1% after several hours), and brown, insoluble side products are formed. Thus, the thermal decomposition of **2** appears to take place at a faster rate than the reaction with $Fe(CO)_5$.

However, the reaction of **2** with $Fe_2(CO)_9$ gave higher yields of **3** (~10%). Diiron nonacarbonyl is known to be a good source of coordinatively unsaturated $Fe(CO)_4$ units in solution, especially in heat-induced metal carbonyl reactions.[30] Compounds **3** or **6** probably form via the coordination of a proximal phosphazene skeletal nitrogen atom to an iron tetracarbonyl fragment, with concurrent loss of two carbonyl ligands to yield the metal–metal bonded framework. As in **2** or **5**, each of the iron atoms in **3** or **6** possesses a closed-shell electronic configuration and obeys the 18-electron rule.

Mixed-Metal Cluster System. If the above argument is correct, it might be supposed that **2** would react with $Ru_3(CO)_{12}$ to yield a mixed Fe–Ru metal cluster, similar in structure to **3**. This does occur. The interaction of **2** with $Ru_3(CO)_{12}$ in boiling heptane provided a low yield (5%) of **7**. The spectral and analytical data are consistent with the formulation of **7** shown, with the two iron atoms remaining covalently bound to the phosphazenyl phosphorus atom and the ruthenium atom coordinatively bonded to the ring nitrogen atom. Compound **7** is an air-stable, violet-red crystalline solid. The solution properties are similar to those of **3** and **6**.

The formation of **7** was accompanied by the formation of $FeRu_2(CO)_{12}$. This suggests that expulsion of an $Fe(CO)_4$ unit from **2** must also occur in this reaction. However, ~80% of **2** was recovered unchanged; hence, this side reaction is of little consequence, at least under the reaction conditions employed.

Spectroscopic Characterization. (a) Infrared Spectra. The solution infrared spectroscopic data for the carbonyl regions of each compound are summarized in Table I. The data are consistent with the indicated structures. Compounds **3**, **6**, and **7** show a broad absorbance ~1870 cm^{-1} that corresponds to the bridging carbonyl group in these structures. No bridging carbonyl ab-

(30) King, R. B. *Prog. Inorg. Chem.* **1972**, *15*, 287.

Table V. Bond Angles (deg) for **2**

	A	B		A	B
Fe(2)–Fe(1)–P(1)	52.1 (1)	50.8 (1)	C(1)–Fe(1)–C(2)	88 (1)	89.1 (8)
Fe(1)–Fe(2)–P(1)	52.9 (1)	51.9 (1)	C(1)–Fe(1)–C(3)	177 (1)	179 (1)
Fe(1)–P(1)–Fe(2)	75.1 (2)	77.3 (2)	C(1)–Fe(1)–C(4)	91 (1)	89.8 (9)
Fe(1)–P(1)–N(1)	114.8 (6)	116.8 (6)	C(2)–Fe(1)–C(3)	89 (1)	90.6 (9)
Fe(1)–P(1)–N(3)	116.1 (6)	114.7 (6)	C(2)–Fe(1)–C(4)	111 (1)	108.8 (9)
Fe(2)–P(1)–N(1)	118.5 (6)	115.6 (6)	C(3)–Fe(1)–C(4)	90 (1)	91.7 (9)
Fe(2)–P(1)–N(3)	117.7 (6)	116.4 (6)	C(5)–Fe(2)–C(6)	87 (1)	87.5 (8)
Fe(2)–Fe(1)–C(1)	87.6 (7)	89.6 (5)	C(5)–Fe(2)–C(7)	174 (1)	174 (1)
Fe(2)–Fe(1)–C(2)	145.6 (8)	155.4 (7)	C(5)–Fe(2)–C(8)	93 (1)	88 (1)
Fe(2)–Fe(1)–C(3)	94.3 (7)	90.1 (6)	C(6)–Fe(2)–C(7)	87 (1)	87.6 (9)
Fe(2)–Fe(1)–C(4)	100.4 (9)	95.7 (6)	C(6)–Fe(2)–C(8)	106 (1)	112 (1)
Fe(1)–Fe(2)–C(5)	90.0 (8)	93.1 (6)	C(7)–Fe(2)–C(8)	91 (1)	91 (1)
Fe(1)–Fe(2)–C(6)	155.2 (8)	150.4 (7)	N(1)–P(1)–N(3)	110.6 (8)	112.1 (8)
Fe(1)–Fe(2)–C(7)	94.1 (8)	92.7 (7)	N(1)–P(2)–N(2)	120.2 (8)	120.1 (9)
Fe(1)–Fe(2)–C(8)	98.5 (8)	97.9 (7)	N(2)–P(3)–N(3)	121.8 (7)	119.2 (9)
P(1)–Fe(1)–C(1)	90.3 (6)	88.5 (5)	P(1)–N(1)–P(2)	126.1 (9)	124.4 (10)
P(1)–Fe(1)–C(2)	96.8 (8)	104.7 (7)	P(2)–N(2)–P(3)	115.8 (9)	119.9 (12)
P(1)–Fe(1)–C(3)	89.2 (8)	90.2 (6)	P(1)–N(3)–P(3)	125.0 (10)	123.5 (9)
P(1)–Fe(1)–C(4)	152.3 (9)	146.4 (6)	Cl(1)–P(2)–Cl(2)	99.8 (4)	99.2 (4)
P(1)–Fe(2)–C(5)	90.1 (8)	92.4 (7)	Cl(3)–P(3)–Cl(4)	99.9 (3)	100.0 (4)
P(1)–Fe(2)–C(6)	102.5 (8)	98.5 (7)	Cl(1)–P(2)–N(1)	111.4 (6)	110.1 (7)
P(1)–Fe(2)–C(7)	88.7 (8)	91.4 (9)	Cl(1)–P(2)–N(2)	107.1 (6)	106.6 (7)
P(1)–Fe(2)–C(8)	151.2 (8)	149.7 (7)	Cl(2)–P(2)–N(1)	110.2 (7)	110.1 (6)
Fe(1)–C(1)–O(1)	172 (2)	175 (1)	Cl(2)–P(2)–N(2)	106.1 (6)	108.6 (8)
Fe(1)–C(2)–O(2)	179 (2)	177 (2)	Cl(3)–P(3)–N(2)	106.8 (6)	109.4 (8)
Fe(1)–C(3)–O(3)	176 (2)	175 (2)	Cl(3)–P(3)–N(3)	108.9 (6)	109.2 (7)
Fe(1)–C(4)–O(4)	174 (2)	176 (2)	Cl(4)–P(3)–N(2)	105.0 (6)	106.7 (7)
Fe(2)–C(5)–O(5)	176 (2)	175 (2)	Cl(4)–P(3)–N(3)	112.1 (7)	110.7 (6)
Fe(2)–C(6)–O(6)	179 (2)	178 (2)			
Fe(2)–C(7)–O(7)	175 (2)	177 (2)			
Fe(2)–C(8)–O(8)	173 (2)	175 (3)			

Table VI. Fractional Atomic Positional Parameters for **2**

	A			B		
	x	*y*	*z*	*x*	*y*	*z*
Fe(1)	0.1017 (3)	0.0	0.8986 (2)	−0.6392 (3)	0.5077 (2)	0.7346 (1)
Fe(2)	0.3073 (3)	0.0817 (2)	0.8029 (1)	−0.6047 (4)	0.5968 (2)	0.5983 (2)
Cl(1)	−0.0823 (8)	0.3559 (3)	0.8340 (3)	−0.8092 (7)	0.2467 (3)	0.5264 (4)
Cl(2)	−0.2755 (8)	0.2527 (5)	0.9470 (4)	−0.7863 (8)	0.3626 (6)	0.3768 (4)
Cl(3)	0.1715 (9)	0.2100 (4)	1.1598 (3)	−0.1943 (8)	0.4030 (5)	0.4760 (4)
Cl(4)	0.4064 (8)	0.3137 (4)	1.0695 (4)	−0.2140 (8)	0.2790 (4)	0.6184 (4)
P(1)	0.1598 (6)	0.1324 (3)	0.9020 (3)	−0.5810 (5)	0.4674 (3)	0.6150 (3)
P(2)	−0.0466 (6)	0.2649 (3)	0.9150 (3)	−0.6818 (5)	0.3437 (3)	0.4988 (3)
P(3)	0.2148 (6)	0.2411 (3)	1.0404 (3)	−0.3534 (6)	0.3621 (3)	0.5534 (3)
N(1)	0.004 (2)	0.1900 (9)	0.8695 (9)	−0.720 (2)	0.4144 (9)	0.558 (1)
N(2)	0.067 (2)	0.2977 (8)	1.0022 (9)	−0.501 (2)	0.316 (1)	0.497 (1)
N(3)	0.261 (2)	0.1663 (9)	0.9923 (9)	−0.395 (2)	0.430 (1)	0.615 (1)
O(1)	0.383 (2)	−0.037 (1)	1.0281 (9)	−0.285 (2)	0.5215 (9)	0.8045 (8)
O(2)	−0.103 (2)	0.002 (1)	1.0414 (9)	−0.642 (2)	0.3618 (9)	0.841 (1)
O(3)	−0.207 (2)	0.034 (1)	0.780 (1)	−0.990 (2)	0.484 (1)	0.6868 (9)
O(4)	0.133 (3)	−0.157 (1)	0.823 (1)	−0.709 (3)	0.645 (1)	0.856 (1)
O(5)	0.033 (2)	0.109 (1)	0.663 (1)	−0.250 (2)	0.626 (1)	0.645 (1)
O(6)	0.459 (3)	0.225 (1)	0.738 (1)	−0.535 (2)	0.605 (1)	0.4190 (8)
O(7)	0.603 (2)	0.069 (1)	0.935 (1)	−0.957 (2)	0.583 (1)	0.528 (1)
O(8)	0.428 (2)	−0.059 (1)	0.718 (1)	−0.674 (3)	0.757 (1)	0.675 (1)
C(1)	0.282 (3)	−0.019 (1)	0.978 (1)	−0.417 (2)	0.517 (1)	0.7780 (9)
C(2)	0.020 (3)	0.000 (1)	0.985 (1)	−0.640 (2)	0.421 (1)	0.804 (1)
C(3)	0.088 (3)	0.021 (1)	0.822 (1)	−0.857 (2)	0.496 (1)	0.708 (1)
C(4)	0.113 (3)	−0.094 (1)	0.856 (2)	−0.678 (3)	0.595 (1)	0.814 (1)
C(5)	0.133 (3)	0.099 (2)	0.718 (1)	−0.378 (3)	0.613 (1)	0.631 (1)
C(6)	0.401 (3)	0.170 (2)	0.763 (1)	−0.564 (2)	0.603 (1)	0.488 (1)
C(7)	0.494 (3)	0.075 (1)	0.891 (1)	−0.822 (3)	0.587 (2)	0.557 (1)
C(8)	0.383 (3)	−0.002 (1)	0.747 (1)	−0.640 (3)	0.697 (1)	0.644 (1)

sorbances were detected for **2** or **5** in solution. The infrared spectral data for **5** and **6** are virtually identical with the values obtained for **2** and **3**, respectively. On the basis of this comparison, it is reasonable to assign similar structures to the metal frameworks in the corresponding trimeric and tetrameric metallophosphazenes.

The solid-state (KBr pellet) infrared spectrum for each compound was in agreement with the solution spectrum. Thus, no fluxionality was detected between bridging and nonbridging carbonyls following dissolution. This feature contrasts with the behavior of the methylene-bridged dimer $Fe_2(CO)_8CH_2$.[28] In solution $Fe_2(CO)_8CH_2$ shows evidence for only terminal carbonyl groups, whereas in the solid state, the compound contains two bridging groups. The phosphazene may serve to hold the carbonyl groups more tightly to the iron atoms in **2** through an electron-withdrawing inductive effect.

In addition to the carbonyl bands the spectra of the phosphazenes contain a broad absorbance in the 1100–1250 cm^{-1} range, characteristic of cyclic phosphazene compounds (P=N vibrations).

(b) ^{31}P NMR Spectra. The ^{31}P NMR data for each compound are listed in Table I. The spectra for **2**, **3**, and **7** are depicted in Figure 1. All the metallophosphazenes show a large downfield chemical shift for the phosphorus atom attached to the transition

Table VII. Bond Lengths (Å) for 3

	A	B
Fe(1)-Fe(2)	2.621 (4)	2.618 (4)
Fe(1)-Fe(3)	2.670 (4)	2.675 (5)
Fe(2)-Fe(3)	2.689 (5)	2.679 (5)
Fe(1)-P(1)	2.206 (6)	2.171 (6)
Fe(2)-P(1)	2.197 (6)	2.186 (6)
Fe(3)-N(1)	2.07 (2)	2.01 (2)
Fe(1)-C(1)	2.01 (2)	2.01 (2)
Fe(2)-C(1)	1.98 (2)	1.94 (2)
Fe(1)-C(2)	1.74 (3)	1.78 (2)
Fe(1)-C(3)	1.77 (3)	1.84 (3)
Fe(1)-C(4)	1.80 (3)	1.75 (3)
Fe(2)-C(5)	1.83 (2)	1.81 (2)
Fe(2)-C(6)	1.77 (2)	1.79 (2)
Fe(2)-C(7)	1.80 (3)	1.76 (3)
Fe(3)-C(8)	1.76 (3)	1.84 (2)
Fe(3)-C(9)	1.77 (2)	1.81 (3)
Fe(3)-C(10)	1.74 (3)	1.73 (2)
P(2)-Cl(1)	2.010 (8)	1.978 (8)
P(2)-Cl(2)	2.010 (9)	1.986 (8)
P(3)-Cl(3)	1.97 (1)	1.978 (9)
P(3)-Cl(4)	1.990 (9)	1.98 (1)
P(1)-N(1)	1.65 (2)	1.67 (2)
P(1)-N(3)	1.60 (2)	1.60 (2)
P(2)-N(1)	1.56 (2)	1.60 (2)
P(3)-N(3)	1.59 (2)	1.56 (2)
P(2)-N(2)	1.54 (2)	1.58 (2)
P(3)-N(2)	1.58 (2)	1.59 (2)
C(1)-O(1)	1.18 (3)	1.19 (3)
C(2)-O(2)	1.17 (3)	1.16 (3)
C(3)-O(3)	1.18 (4)	1.15 (3)
C(4)-O(4)	1.15 (4)	1.17 (3)
C(5)-O(5)	1.13 (3)	1.17 (3)
C(6)-O(6)	1.13 (3)	1.18 (3)
C(7)-O(7)	1.16 (3)	1.14 (3)
C(8)-O(8)	1.16 (3)	1.13 (3)
C(9)-O(9)	1.14 (3)	1.17 (3)
C(10)-O(10)	1.17 (3)	1.17 (3)
	Solvent	
C(O1)-C(O2)	1.38 (7)	
C(O2)-C(O3)	1.37 (4)	
C(O3)-C(O4)	1.38 (5)	
C(O4)-C(O5)	1.32 (5)	

metals. This pronounced deshielding effect is partly a consequence of the constrained metal–phosphorus–metal bond angle, which is in the range of 70–80° (see X-ray data). This effect was also observed for metal–metal bonded metallofluorophosphazenes ($N_3P_3F_4M_2Cp_2(CO)_3$, M = Fe or Ru).[25,26]

The range of chemical shifts observed for the $P(Cl)_2$ resonances is between −13 and +30 ppm. The lower field resonances within the $P(Cl)_2$ region for 3 and 7 were assigned to the phosphorus adjacent to the metal-bound nitrogen (Figure 1b,c). Coordinative electron donation by this nitrogen atom would cause a deshielding of the neighboring phosphorus atom.

Each phosphorus atom in **5** and **6** shows a measurable coupling to the adjacent phosphorus atoms in the molecule (coupling constants are listed in Table I). However, no 1,5-coupling interactions were observed for the cyclic tetramers. In **5**, the two phosphorus atoms adjacent to the metal-bound phosphorus are chemically equivalent. As expected, all four phosphorus environments are different in **6**. This is consistent with a triiron cluster arrangement analogous to the configuration discussed for **3**.

(c) Mössbauer Spectra. Mössbauer spectroscopy allows the identification of different iron environments present in a compound. The data for the new iron-containing phosphazenes are listed in Table II. The stack-plotted spectra corresponding to compounds **2**, **3**, and **7** are shown in Figure 2.

The Mössbauer spectrum of **3** (Figure 2b) consists of two doublets in the ratio of 2:1. The right half of each doublet occurs at approximately the same position, resulting in a coincident single absorbance. The indicated presence of two different iron species in a 2:1 ratio is consistent with the X-ray diffraction results and the elemental analysis.

The Mössbauer spectrum of **7** (Figure 2c) consisted of one doublet that is coincident with the doublet in the spectrum of **2** and with the larger of the two doublets in the spectrum of **3**. It thus corresponds to the phosphorus-bound iron species. The isomer shift and the quadrupole splitting parameters for **7** (see Table II) are not identical with those for **2** or **3**, but the changes are slight and the spectrum results from two iron atoms in equivalent positions. Thus, the ruthenium atom must be coordinated to the nitrogen atom of the phosphazene ring. This is consistent with the X-ray diffraction results and the other spectroscopic data.

The spectra of **2** and **5** are similar, as are the spectra of **3** and **6**. This further confirms the similarity in structure of the trimeric and tetrameric metallophosphazene analogues.

The line widths measured for all the species are essentially equal to the minimum instrumental line width of ~0.230 mm/s; thus, all the samples are homogeneous. The isomer shifts did not allow the unambiguous assignment of valence and spin values to the iron species. However, high-spin ferrous species can be ruled out.

X-ray Structure Analyses: General Information. A single-crystal X-ray structure determination was carried out for the cyclic trimeric metallophosphazenes **2**, **3**, and **7**. The main crystallographic details are summarized in Table III. Bond lengths, bond angles, and atomic positional parameters are listed in Tables IV–XII.[31] The tables of thermal parameters,[32] root-mean-square displacements, and F_o and F_c values are available as supplementary material. Labeled ORTEP drawings for each structure are shown in Figures 3–5 (only one of the unique molecules for each acentric structure is shown).

Structure of 2. The structure of **2** was solved in the acentric space group $P2_1$. A comparison of the data for each unique molecule revealed no significant differences beyond those that might be expected from crystal-packing distortions.

The two iron atoms in **2** form a three-membered spiro ring, with a metal-bound phosphorus atom at the spiro juncture. The phosphazene ring in **2** is essentially planar ($\chi^2 = 26$) and the dihedral angle between the Fe(1)–Fe(2)–P(1) plane and the plane of the phosphazene ring is 89.3°.[33] The plane defined by the three-membered spiro ring passes through the distal nitrogen N(2) (with less than 1° deviation).

Each iron atom in **2** is connected to four terminal carbonyl groups (Figure 3). The configuration about each iron atom is that of a distorted octahedron. The idealized C_{2v} symmetry in **2** is disrupted by crystal-packing forces. Even so, the carbonyl groups on one iron atom virtually eclipse those on the adjoining iron atom. In part, this may explain the somewhat longer Fe–Fe bond length (2.746 Å) in **2**, compared to other related neutral dimetallo complexes. For example, the Fe–Fe distance in the diiron phosphazene $N_3P_3F_4Fe_2Cp_2(CO)_3$ is 2.593 Å.[25] Other related compounds include $Fe_2(PPh_2)_2(CO)_6$, 2.623 Å,[34] and $Fe_2(CO)_8CH_2$, 2.507 Å.[28] The compound described by Clegg,[35] $Fe_2(CO)_6[P(CF_3)_2]_2$, possesses a long Fe–Fe bond of 2.819 Å. Clegg rationalized the long Fe–Fe distance by considering the effects of the electron-withdrawing CF_3 groups on the bonding orbitals in that compound. For compound **2**, the somewhat long Fe–Fe distance can be attributed to both the electronegative phosphazene ring and the eclipsed carbonyl groups. For structurally related dimers, a "bent" metal–metal bond has been proposed that is conceptually veiwed as completing the approximately octahedral coordination about each metal atom.[36,37]

(31) The number in parentheses following each numerical entry in Tables IV–XII represents the estimated standard deviation (corresponding to the uncertainty in the last digit) of the value.

(32) The form of the anisotropic thermal parameter is $\exp[-2\pi^2(U_{11a}{}^{*2}h^2 + U_{22}b^{*2}k^2 + U_{33}c^{*2}l^2 + 2U_{12}a^*b^*hk + 2U_{13}a^*c^*hl + 2U_{23}b^*c^*kl)]$. The units of the values are in 10^3 Å^2.

(33) This value, and all subsequent values for the acentric structures, represents an average of the values from the two unique molecules within the structure.

(34) Collman, J. P.; Rothrock, R. K.; Finke, R. G.; Moore, E. J.; Rose-Munch, F. *Inorg. Chem.* **1982**, *21*, 146.

(35) Clegg, W. *Inorg. Chem.* **1976**, *15*, 1609.

Table VIII. Bond Angles (deg) for **3**

	A	B		A	B
Fe(2)–Fe(1)–Fe(3)	61.1 (1)	60.8 (1)	Fe(1)–C(1)–O(1)	138 (2)	135 (2)
Fe(1)–Fe(2)–Fe(3)	60.4 (1)	60.6 (1)	Fe(2)–C(1)–O(1)	140 (2)	142 (2)
Fe(1)–Fe(3)–Fe(2)	58.6 (1)	58.5 (1)	Fe(1)–C(1)–Fe(2)	82.0 (9)	82.9 (8)
Fe(2)–Fe(1)–P(1)	53.3 (2)	53.3 (2)	Fe(1)–C(2)–O(2)	177 (2)	175 (3)
Fe(1)–Fe(2)–P(1)	53.6 (2)	52.8 (2)	Fe(1)–C(3)–O(3)	176 (3)	173 (3)
Fe(3)–Fe(1)–P(1)	65.3 (2)	64.0 (2)	Fe(1)–C(4)–O(4)	177 (2)	176 (2)
Fe(3)–Fe(2)–P(1)	65.1 (2)	63.7 (2)	Fe(2)–C(5)–O(5)	175 (2)	175 (2)
Fe(1)–Fe(3)–N(1)	80.6 (5)	82.1 (5)	Fe(2)–C(6)–O(6)	176 (2)	179 (2)
Fe(2)–Fe(3)–N(1)	80.5 (5)	81.8 (5)	Fe(2)–C(7)–O(7)	178 (2)	177 (2)
Fe(1)–P(1)–Fe(2)	73.0 (2)	73.9 (2)	Fe(3)–C(8)–O(8)	176 (2)	171 (2)
Fe(1)–P(1)–N(1)	106.2 (7)	107.7 (6)	Fe(3)–C(9)–O(9)	178 (2)	176 (2)
Fe(1)–P(1)–N(3)	125.2 (7)	126.0 (7)	Fe(3)–C(10)–O(10)	173 (2)	172 (2)
Fe(2)–P(1)–N(1)	107.3 (7)	106.7 (7)	C(1)–Fe(1)–C(2)	177 (1)	174 (1)
Fe(2)–P(1)–N(3)	127.7 (8)	126.0 (7)	C(1)–Fe(1)–C(3)	84 (1)	84 (1)
Fe(3)–N(1)–P(1)	90.4 (7)	89.6 (7)	C(1)–Fe(1)–C(4)	87 (1)	89 (1)
Fe(3)–N(1)–P(2)	142 (1)	144 (1)	C(2)–Fe(1)–C(3)	94 (1)	91 (1)
Fe(2)–Fe(1)–C(1)	48.6 (7)	47.3 (6)	C(2)–Fe(1)–C(4)	95 (1)	96 (1)
Fe(1)–Fe(2)–C(1)	49.4 (7)	49.8 (6)	C(3)–Fe(1)–C(4)	97 (1)	102 (1)
Fe(3)–Fe(1)–C(1)	97.5 (8)	95.7 (7)	C(1)–Fe(2)–C(5)	84 (1)	84 (1)
Fe(3)–Fe(2)–C(1)	97.5 (8)	97.5 (7)	C(1)–Fe(2)–C(6)	177 (1)	176 (1)
P(1)–Fe(1)–C(1)	96.4 (7)	96.0 (6)	C(1)–Fe(2)–C(7)	86 (1)	86 (1)
P(1)–Fe(2)–C(1)	97.4 (7)	97.8 (7)	C(5)–Fe(2)–C(6)	94 (1)	92 (1)
Fe(2)–Fe(1)–C(2)	131.9 (9)	133.3 (8)	C(5)–Fe(2)–C(7)	101 (1)	105 (1)
Fe(2)–Fe(1)–C(3)	119.8 (9)	118.4 (8)	C(6)–Fe(2)–C(7)	94 (1)	96 (1)
Fe(2)–Fe(1)–C(4)	111.4 (8)	110.7 (7)	C(8)–Fe(3)–C(9)	101 (1)	92 (1)
Fe(3)–Fe(1)–C(2)	81 (1)	80.8 (9)	C(8)–Fe(3)–C(10)	91 (1)	95 (1)
Fe(3)–Fe(1)–C(3)	101 (1)	98.1 (9)	C(9)–Fe(3)–C(10)	96 (1)	92 (1)
Fe(3)–Fe(1)–C(4)	162.3 (8)	160.0 (7)	N(1)–P(1)–N(3)	111 (1)	110.9 (9)
P(1)–Fe(1)–C(2)	85.2 (9)	87.4 (8)	N(1)–P(2)–N(2)	115 (1)	115 (1)
P(1)–Fe(1)–C(3)	166 (1)	162 (1)	N(2)–P(3)–N(3)	117 (1)	118 (1)
P(1)–Fe(1)–C(4)	97.1 (8)	96.2 (7)	P(1)–N(1)–P(2)	127 (1)	126 (1)
Fe(1)–Fe(2)–C(5)	118.2 (7)	117.3 (7)	P(2)–N(2)–P(3)	123 (1)	123 (1)
Fe(1)–Fe(2)–C(6)	132.9 (7)	132.0 (7)	P(1)–N(3)–P(3)	123 (1)	125 (1)
Fe(1)–Fe(2)–C(7)	110.9 (7)	110.4 (8)	Cl(1)–P(2)–Cl(2)	99.7 (4)	102.9 (4)
Fe(3)–Fe(2)–C(5)	97.3 (9)	93.6 (7)	Cl(3)–P(3)–Cl(4)	102.2 (4)	101.4 (4)
Fe(3)–Fe(2)–C(6)	83.5 (7)	81.4 (7)	Cl(1)–P(2)–N(1)	111.2 (7)	108.9 (7)
Fe(3)–Fe(2)–C(7)	161.5 (7)	161.3 (8)	Cl(1)–P(2)–N(2)	108.7 (7)	111.1 (7)
P(1)–Fe(2)–C(5)	162.4 (9)	157.3 (8)	Cl(2)–P(2)–N(1)	109.0 (7)	110.2 (7)
P(1)–Fe(2)–C(6)	85.3 (7)	85.5 (7)	Cl(2)–P(2)–N(2)	112.0 (8)	107.5 (8)
P(1)–Fe(2)–C(7)	96.5 (7)	97.6 (8)	Cl(3)–P(3)–N(2)	106.6 (7)	108.8 (7)
Fe(1)–Fe(3)–C(8)	157.0 (9)	161.1 (8)	Cl(3)–P(3)–N(3)	110.9 (8)	111.7 (8)
Fe(1)–Fe(3)–C(9)	102.1 (7)	106.7 (9)	Cl(4)–P(3)–N(2)	109.7 (8)	106.9 (8)
Fe(1)–Fe(3)–C(10)	86.4 (9)	83.2 (8)	Cl(4)–P(3)–N(3)	109.1 (8)	108.7 (8)
Fe(2)–Fe(3)–C(8)	98.4 (9)	102.6 (8)			
Fe(2)–Fe(3)–C(9)	160.4 (8)	165.2 (9)	Solvent		
Fe(2)–Fe(3)–C(10)	86.0 (9)	87.6 (8)	C(O1)–C(O2)–C(O3)	124 (2)	
N(1)–Fe(3)–C(8)	98 (1)	97.6 (9)	C(O3)–C(O2)–C(O3)^a	113 (4)	
N(1)–Fe(3)–C(9)	94.1 (9)	96 (1)	C(O2)–C(O3)–C(O4)	124 (3)	
N(1)–Fe(3)–C(10)	165 (1)	165 (1)	C(O3)–C(O4)–C(O5)	117 (4)	
			C(O4)–C(O5)–C(O4)^a	124 (6)	

^{a}Symmetry related by $-x$, $-y$, z.

The skeletal phosphorus atoms in cyclic phosphazenes usually occupy a distorted tetrahedral geometry, with a ring angle usually near 120° and an exocyclic angle near 100°.[38] In **2**, the Fe(1)–P(1)–Fe(2) angle is 76.2° and the N(1)–P(1)–N(3) angle is constricted to 111.4°. Although the narrowing of the endocyclic angle has been detected for other substituted phosphazenes,[39] the marked constriction of the exocyclic angle is peculiar to metallophosphazenes that possess three-membered spiro ring arrangements.[24,25] The other endocyclic angles centered at P(2) and P(3) in **2** are similar to those in $(NPCl_2)_3$ (~120°).[38]

Another feature common to many unsymmetrically substituted cyclophosphazenes is an alternation in longer and shorter bonds for the P–N bonds located at increasing distances from the substitution site.[24,39] This effect was also found for compound **2**. The two P–N bonds proximal to the iron atoms are the longest (mean distance = 1.63 Å). The adjacent pair of P–N bonds are the shortest (mean distance = 1.54 Å) and those furthest from the iron atoms were of intermediate length (mean distance = 1.59 Å). The length of the P–N bonds furthest from P(1) are very similar to those found in $(NPCl_2)_3$ (~1.58 Å).[38] This alternation in bond lengths has been attributed to variations in the bonding within the phosphazene ring, caused by the less electronegative substitutents at P(1).

Other structural features of **2** include the following: (1) the endocyclic bond angles centered at N(1) and N(3) average 124.8°, whereas the distal angle centered at N(2) is contracted (117.8°); (2) the exocyclic Cl–P(2 or 3)–Cl angles (average 99.7°) are similar to those found in $(NPCl_2)_3$;[38,40,41] (3) the acute P(1)–Fe(1)–Fe(2) and P(1)–Fe(2)–Fe(1) angles average 51.9°; (4) the Fe(1)–P(1) and Fe(2)–P(1) bond lengths (average 2.226 Å) are in agreement with values quoted for related dimers.[42]

(36) Dahl, L. F.; Costello, W. R.; King, R. B. *J. Am. Chem. Soc.* **1968**, *90*, 5422.
(37) Teo, B. K.; Hall, M. B.; Fenske, R. F.; Dahl, L. F. *Inorg. Chem.* **1975**, *14*, 3103.
(38) Allcock, H. R. "Phosphorus-Nitrogen Compounds"; Academic Press: New York, 1972.
(39) Allcock, H. R.; Ritchie, R. J.; Harris, P. J. *Inorg. Chem.* **1980**, *19*, 2483.
(40) Giglio, E. *Ric. Sci.* **1960**, *30*, 721.
(41) Wilson, A.; Carrol, D. F. *J. Chem. Soc.* **1960**, 2548.
(42) Ginsburg, R. E.; Rothrock, R. K.; Finke, R. G.; Collman, J. P.; Dahl, L. F. *J. Am. Chem. Soc.* **1979**, *101*, 6550.

Table IX. Fractional Atomic Positional Parameters for **3**

	A			B		
	x	*y*	*z*	*x*	*y*	*z*
Fe(1)	0.4420 (1)	0.3428 (1)	0.0	0.1581 (1)	−0.0576 (1)	−0.0576 (4)
Fe(2)	0.5172 (1)	0.2642 (1)	−0.0056 (5)	0.2319 (1)	0.0218 (1)	−0.0353 (5)
Fe(3)	0.4472 (1)	0.2757 (1)	−0.2473 (5)	0.2229 (1)	−0.0528 (1)	0.1950 (5)
Cl(1)	0.3855 (2)	0.1126 (2)	−0.2185 (8)	0.3847 (2)	−0.1085 (3)	0.1954 (9)
Cl(2)	0.2925 (2)	0.1993 (3)	−0.248 (1)	0.3055 (2)	−0.2088 (2)	0.1536 (9)
Cl(3)	0.3546 (3)	0.1350 (3)	0.3768 (9)	0.3920 (3)	−0.0753 (4)	−0.349 (1)
Cl(4)	0.2844 (3)	0.2366 (3)	0.282 (1)	0.3222 (4)	−0.1778 (3)	−0.4282 (9)
P(1)	0.4290 (2)	0.2541 (2)	0.0524 (8)	0.2467 (2)	−0.0648 (2)	−0.0990 (8)
P(2)	0.3552 (2)	0.1790 (2)	−0.1048 (7)	0.3264 (2)	−0.1373 (2)	0.0548 (6)
P(3)	0.3492 (2)	0.1918 (2)	0.2121 (7)	0.3301 (2)	−0.1201 (2)	−0.2649 (7)
N(1)	0.3982 (6)	0.2274 (7)	−0.102 (3)	0.2748 (6)	−0.0955 (7)	0.057 (2)
N(2)	0.3343 (8)	0.1601 (7)	0.056 (2)	0.3507 (7)	−0.1508 (8)	−0.111 (3)
N(3)	0.4029 (8)	0.2302 (8)	0.210 (2)	0.2753 (7)	−0.0861 (7)	−0.256 (2)
O(1)	0.5568 (7)	0.3765 (7)	0.092 (2)	0.1189 (6)	0.0567 (6)	−0.129 (2)
O(2)	0.3248 (8)	0.3453 (7)	−0.082 (2)	0.1589 (7)	−0.1766 (7)	0.014 (2)
O(3)	0.4635 (9)	0.4501 (9)	−0.156 (3)	0.0461 (8)	−0.0432 (8)	0.087 (3)
O(4)	0.4251 (8)	0.3825 (8)	0.321 (2)	0.1252 (8)	−0.0701 (8)	−0.382 (3)
O(5)	0.6192 (7)	0.2850 (7)	−0.189 (2)	0.2068 (7)	0.1198 (7)	0.163 (2)
O(6)	0.5129 (6)	0.1469 (6)	−0.082 (2)	0.3493 (6)	0.0216 (6)	0.070 (2)
O(7)	0.5622 (7)	0.2424 (7)	0.310 (2)	0.2533 (7)	0.0680 (7)	−0.341 (2)
O(8)	0.4875 (8)	0.1866 (8)	−0.449 (3)	0.3053 (7)	−0.0068 (7)	0.416 (2)
O(9)	0.3539 (7)	0.3132 (7)	−0.437 (2)	0.1892 (8)	−0.1486 (8)	0.392 (3)
O(10)	0.5241 (7)	0.3557 (7)	−0.380 (2)	0.1377 (7)	0.0181 (7)	0.326 (2)
C(1)	0.524 (1)	0.344 (1)	0.049 (4)	0.1540 (9)	0.0251 (9)	−0.091 (3)
C(2)	0.372 (1)	0.343 (1)	−0.051 (4)	0.159 (1)	−0.129 (1)	−0.007 (3)
C(3)	0.456 (1)	0.408 (1)	−0.089 (4)	0.091 (1)	−0.048 (1)	0.040 (4)
C(4)	0.431 (1)	0.368 (1)	0.194 (4)	0.1379 (9)	−0.0670 (9)	−0.251 (3)
C(5)	0.582 (1)	0.277 (1)	−0.113 (3)	0.2153 (8)	0.0799 (9)	0.090 (3)
C(6)	0.5149 (9)	0.1931 (9)	−0.057 (3)	0.3027 (9)	0.0218 (9)	0.029 (3)
C(7)	0.5436 (9)	0.2508 (9)	0.187 (3)	0.245 (1)	0.0512 (9)	−0.219 (3)
C(8)	0.473 (1)	0.222 (1)	−0.366 (4)	0.275 (1)	−0.0284 (9)	0.336 (3)
C(9)	0.3903 (9)	0.2992 (8)	−0.361 (3)	0.204 (1)	−0.111 (1)	0.316 (3)
C(10)	0.496 (1)	0.322 (1)	−0.322 (3)	0.1691 (9)	−0.0129 (9)	0.269 (3)
			Solvent			
C(O1)	0.5	0.0	0.015 (6)			
C(O2)	0.5	0.0	0.0176 (5)			
C(O3)	0.480 (1)	0.043 (1)	0.265 (4)			
C(O4)	0.483 (2)	0.045 (1)	0.426 (5)			
C(O5)	0.5	0.0	0.498 (8)			

Structures of 3 and 7. The structures of **3**[43] and **7** were solved in the $P4_2$ space group. In each case the results of refinement of the intensity data revealed the presence of two toluene molecules per unit cell. The carbon atoms of the toluene molecule were located (Tables IX and XII) and were refined isotropically. (The solvent molecule was situated on a twofold axis of symmetry).

The structures of **3** and **7** are similar and are shown in Figures 4 and 5 (only one of the unique molecules for each structure is shown). The cluster unit, defined by the three metal atoms and the P(1)–N(1) edge of the phosphazene ring, forms a wedge-shaped, irregular polyhedron. The overall metallic framework in these compounds is structurally similar to that of the known compound $Fe_3(CO)_{12}$, **8**.[29] $Fe_2Ru(CO)_{12}$ is also believed to have a molecular structure similar to that of $Fe_3(CO)_{12}$.[44] Thus, **8**

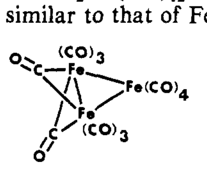

8

provides a useful model for evaluating the influence of the phosphazene ring. In these terms, the phosphazene ring in **3** and **7** functions as a "replacement" for one bridging carbonyl group and one terminal carbonyl group in $Fe_3(CO)_{12}$. Specifically, the bridging phosphazenyl phosphorus in **3** and **7** is analogous to one of the bridging carbonyl groups in **8**, and the phosphazenyl nitrogen is analogous to one of the terminal carbonyl ligands on the remaining iron atom in **8**. Since the phosphorus–iron bonds in **3** and **7** are covalent two-electron bonds and the nitrogen–metal bond results from donation of the ring nitrogen lone pair electrons, the metallic units in **3**, **7**, and **8** are isoelectronic. This configuration is compatible with the observed diamagnetism of **3** and **7**.

The phosphazene ring in compounds **3** and **7** shows some deviation from planarity (**3**, $\chi^2 = 357$ (av); **7**, $\chi^2 = 140$ (av)). The idealized phosphazene plane passes through Fe(3) or Ru (0.18 Å deviation for **3**; 0.19 Å deviation for **7**) and bisects the Fe(1)–Fe(2) linkage. The plane defined by the three metal atoms forms a dihedral angle of 86.6° with the phosphazene ring in **3** (86.4° for **7**) and a dihedral angle of 78.7° (81.5° for **7**) with the P(1)–Fe(1)–Fe(2) plane. The dihedral angle formed by the intersection of the phosphazene plane and the P(1)–Fe(1)–Fe(2) plane in **3** is 87.9° (87.3° for **7**). However, in contrast to the structure of **2**, the P(1)–Fe(1)–Fe(2) plane in **3** forms a 14° (15° for **7**) angle with the imaginary line defined by P(1) and N(2). The result is a substantially distorted tetrahedral configuration about P(1). This effect is caused by the bonding of Fe(1) and Fe(2) to Fe(3) or Ru, which "pulls" the phosphorus-bound iron atoms toward it.

The bond lengths in **3** are given in Table VII. The Fe(1)–Fe(3) distance (2.670 Å)[33] and the Fe(2)–Fe(3) distance (2.689 Å) are in good agreement with the corresponding bond lengths in the model **8** (2.673 Å (av)).[29] The doubly bridged Fe(1)–Fe(2) bond length is 2.621 Å, slightly longer than the corresponding bond in **8** (2.560 Å). A distance of 2.07 Å confirms the existence of

(43) A preliminary X-ray structure determination was carried out on compound **3** on a crystal that was grown from hexane. The space group proved to be $P4_2/n$, and the final *R* factor attained was 0.085. However, the results had indicated that a disordered hexane molecule was contained within the crystal lattice. Therefore, the X-ray structure was redetermined by using a crystal grown from toluene solvent. The preliminary X-ray structure (i.e., the crystal grown from hexane) was reported in the publication given in ref 1.

(44) Yawney, D. B. W.; Stone, F. G. A. *J. Chem. Soc. A* **1969**, 502.

Table X. Bond Lengths (Å) for 7

	A	B
Fe(1)-Fe(2)	2.621 (4)	2.625 (4)
Fe(1)-Ru	2.723 (4)	2.726 (4)
Fe(2)-Ru	2.734 (4)	2.737 (4)
Fe(1)-P(1)	2.180 (6)	2.207 (6)
Fe(2)-P(1)	2.194 (6)	2.189 (6)
Ru-N(1)	2.11 (2)	2.21 (2)
Fe(1)-C(1)	2.01 (2)	2.03 (2)
Fe(2)-C(1)	2.00 (2)	1.98 (2)
Fe(1)-C(2)	1.76 (2)	1.75 (3)
Fe(1)-C(3)	1.77 (2)	1.80 (3)
Fe(1)-C(4)	1.74 (3)	1.82 (3)
Fe(2)-C(5)	1.81 (2)	1.82 (3)
Fe(2)-C(6)	1.78 (2)	1.78 (2)
Fe(2)-C(7)	1.78 (3)	1.77 (2)
Ru-C(8)	1.89 (2)	1.94 (3)
Ru-C(9)	1.87 (3)	1.94 (3)
Ru-C(10)	1.83 (2)	1.86 (3)
P(2)-Cl(1)	1.972 (9)	1.996 (9)
P(2)-Cl(2)	1.985 (9)	2.001 (9)
P(3)-Cl(3)	1.98 (1)	1.98 (1)
P(3)-Cl(4)	1.97 (1)	1.98 (1)
P(1)-N(1)	1.68 (2)	1.65 (2)
P(1)-N(3)	1.56 (2)	1.68 (2)
P(2)-N(1)	1.63 (2)	1.53 (2)
P(3)-N(3)	1.55 (2)	1.59 (2)
P(2)-N(2)	1.58 (2)	1.56 (2)
P(3)-N(2)	1.57 (2)	1.60 (2)
C(1)-O(1)	1.16 (3)	1.17 (3)
C(2)-O(2)	1.18 (3)	1.16 (3)
C(3)-O(3)	1.17 (3)	1.20 (4)
C(4)-O(4)	1.17 (4)	1.10 (4)
C(5)-O(5)	1.14 (3)	1.15 (3)
C(6)-O(6)	1.15 (3)	1.16 (3)
C(7)-O(7)	1.14 (4)	1.19 (3)
C(8)-O(8)	1.19 (3)	1.10 (4)
C(9)-O(9)	1.17 (3)	1.11 (3)
C(10)-O(10)	1.21 (3)	1.16 (4)
	Solvent	
C(O1)-C(O2)	1.40 (9)	
C(O2)-C(O3)	1.36 (5)	
C(O3)-C(O4)	1.36 (7)	
C(O4)-C(O5)	1.44 (6)	

a bond between N(1) and Fe(3).

The bond lengths found for 7 are given in Table X. The Fe(1)-Ru distance is 2.724 Å, and the Fe(2)-Ru distance is 2.736 Å. These bond lengths are longer than the Fe(1)-Fe(3) and Fe(2)-Fe(3) bonds in 3 and are similar to Fe-Ru bond lengths reported for other compounds.[45,46] The doubly bridged Fe(1)-Fe(2) bond length in 7 is 2.623 Å, which is similar to that found for the Fe(1)-Fe(2) bond in 3. The N(1)-Ru bond distance is 2.16 Å, 0.09 Å longer than the N(1)-Fe(3) distance in 3.

For both compounds 3 and 7 the presence of the trimetallic cluster unit causes a disruption in the bond length symmetry in the phosphazene skeleton. Thus, the P(1)-N(1) bond in both compounds is unusually long (1.66 Å in both cases)[38] because of the strain placed on it by the polyhedral enclosure. The remaining P-N bond lengths fall in the range of 1.56-1.60 Å for 3 and 1.57-1.62 Å for 7.

As was found for the diiron phosphazene 2, the smallest endocyclic phosphazene ring angle corresponds to N(1)-P(1)-N(3) (111.0° for 3; 110° for 7). A similarity also exists in the Fe(1)-P(1)-Fe(2) angles (73.4° for 3 and 7). Perhaps the most noteworthy angle is the P(1)-N(1)-P(2) value (126° for 3; 128° for 7). This indicates a structural adjustment by the phosphazene ring to alleviate the distorted trigonal configuration about N(1) (for 3, P(1)-N(1)-Fe(3) is 90.0° and Fe(3)-N(1)-P(2) is 143°; for 7, P(1)-N(1)-Ru is 91.4° and Ru-N(1)-P(2) is 141°). The remaining endocyclic phosphazene angles in 3 lie in the range of 115°-124° (116°-123° for 7). The Cl-P-Cl angles in both compounds (~101°) are similar to those found in $(NPCl_2)_3$.[38]

Experimental Section

Materials. All experimental manipulations were performed under an atmosphere of dry nitrogen (Matheson). Hexachlorocyclotriphosphazene was separated from a mixture of $(NPCl_2)_3$ and $(NPCl_2)_4$ (kindly supplied by Ethyl Corp.) by fractional sublimation. Tetrahydrofuran (Baker) was dried by distillation from potassium benzophenone ketyl. Hexane and heptane (Fisher) were distilled from calcium hydride before use. Collman's reagent ($Na_2Fe(CO)_4 \cdot {}^3/_2$ dioxane), $Fe(CO)_5$, $Fe_2(CO)_9$, and $Ru_3(CO)_{12}$ were commercial products obtained from Alfa-Ventron Corp. or Strem Corp. and were used as received. Two grades of silica gel were used: coarse (60-200 μm mesh, Davison) and fine (32-63 μm, ICN).

Equipment. ^{31}P NMR spectra were recorded by means of a Bruker WP-200 FT NMR spectrometer at 80 MHz. ^1H NMR data were obtained with the same spectrometer at 200 MHz. Infrared spectra were obtained with the use of a Perkin-Elmer 580 grating spectrometer or a Perkin-Elmer 283B infrared spectrometer. Mass spectrometric analyses were performed on a Finnegan 3200 instrument or an AEI MS 902 mass spectrometer. Microanalyses were performed by Galbraith Laboratories, Inc., Knoxville, Tenn.

Mössbauer spectra were recorded with a constant acceleration spectrometer. The samples[47] were mounted on the cold finger of a liquid-nitrogen-cooled cryostat at a temperature of 77 K.[48] Doppler shifts were calibrated with an iron foil, and all velocities are given relative to the centroid of metallic iron at 300 K. All the spectra were matched with Lorentzian-shaped quadrupole pairs, with the isomer shift, the quadrupole splitting, the half-width at half-maximum of the Lorentzians, and the area of the quadrupole pairs as free parameters. A nonlinear least-squares Fortran computer program[49] was used to facilitate the fitting. The solid lines in Figure 2 are the output of the program.

Synthesis of $N_3P_3Cl_4Fe_2(CO)_8$ (2) or $N_4P_4Cl_6Fe_2(CO)_8$ (5) and Isolation of $N_3P_3Cl_4Fe_3(CO)_{10}$ (3) and $N_4P_4Cl_6Fe_3(CO)_{10}$ (6). The following representative procedure also applies to the synthesis of $N_4P_4Cl_6Fe_2(CO)_8$. $Na_2Fe(CO)_4 \cdot {}^3/_2$dioxane (5.0 g, 14.5 mmol) was slurried in THF (100 mL) in a 500-mL Schlenk flask. To this mixture was added $Fe(CO)_5$ (1.9 mL, 14.5 mmol) via syringe, and stirring was maintained for 5 h. A bright red precipitate of $Na_2Fe_2(CO)_8$ was formed. The mixture was cooled to -78 °C with the use of a dry ice/acetone bath, and $(NPCl_2)_3$ (5.0 g, 14.4 mmol) was added slowly as a solution in THF (50 mL). The mixture was then allowed to warm to ambient temperature and was stirred for 12 h. The solvent was removed on a rotary evaporator in a well-ventilated hood to prevent escape of $Fe(CO)_5$ into the laboratory. The reddish solid was shaken with methylene chloride (100 mL) and filtered through a short column of silica gel (coarse). The solvent was again removed by rotary evaporation, and the solid was extracted with methylene chloride (10%)/hexane (90%) and chromatographed on silica gel (coarse) packed with hexane. Elution with hexane brought about the separation of a green band ($Fe_3(CO)_{12}$),[29] followed by a purple band ($N_3P_3Cl_4Fe_3(CO)_{10}$). Finally, elution with 100% methylene chloride yielded an orange band ($N_3P_3Cl_4Fe_2(CO)_8$). After removal of the solvent from each fraction by rotary evaporation, compound 3 was obtained as a purple crystalline material (0.1 g, 1%) and compound 2 was obtained as an orange crystalline solid (1.1 g, 12.5%). Mass spectrum for 2: m/e calcd 611, found 611. Mass spectrum for 3: m/e calcd 722.5598, found 722.5616. Anal. Calcd for $Fe_2Cl_4P_3O_8N_3C_8$: Fe, 18.23; C, 15.69; N, 6.86. Found: Fe, 17.79; C, 15.84; N, 6.87. Anal. Calcd for $Fe_3Cl_4P_3O_{10}N_3C_{10}$: Fe, 23.13; C, 16.58; N, 5.80. Found: Fe, 22.90; C, 16.60; N, 5.30.

The analogous reaction between $N_4P_4Cl_8$ and $Na_2Fe_2(CO)_8$ (equimolar quantities) resulted in the isolation of 5 as a yellow-orange solid (0.035 g, 0.4%) and 6 as a purple-colored solid (trace). Mass spectrum for 5: m/e calcd 725.5496, found 725.5507. Mass spectrum for 6: m/e calcd 837, found 837.

Synthesis of $N_3P_3Cl_4Fe_3(CO)_{10}$ (3) from $N_3P_3Cl_4Fe_2(CO)_8$ (2). Compound 2 (1.0 g, 1.6 mmol) and $Fe_2(CO)_9$ (0.6 g, 1.6 mmol) were placed in a 200-mL airless flask. Freshly distilled hexane (100 mL) was added, and the mixture was heated at reflux for 1 h. After the reaction mixture had cooled to ambient temperature, the dark solution was stirred an additional 5 h and was then applied to a column of silica gel (coarse)

(45) Gilmore, C. J.; Woodward, P. *J. Chem. Soc. A* **1971**, 3453.
(46) Fox, J. R.; Gladfelter, W. L.; Wood, T. G.; Senegal, J. A.; Foreman, T. K.; Geoffroy, G. L.; Tavanaiepour, I.; Day, V. W.; Day, C. S. *Inorg. Chem.* **1981**, *20*, 3214.

(47) Samples were prepared by forming a homogeneous mixture of the solid product with an inert substance (boron nitride) using a mortar and pestle.
(48) Lang, G. *Q. Rev. Biophys.* **1970**, *3*, 1.
(49) See, for example, Chrisman, B. L.; Tumolillo, T. A. *Comput. Phys. Commun.* **1971**, *2*, 322.

Table XI. Bond Angles (deg) for **7**

	A	B		A	B
Fe(2)–Fe(1)–Ru	61.5 (1)	61.5 (1)	Fe(1)–C(1)–O(1)	138 (2)	138 (2)
Fe(1)–Fe(2)–Ru	61.1 (1)	61.1 (1)	Fe(2)–C(1)–O(1)	140 (2)	140 (2)
Fe(1)–Ru–Fe(2)	57.41 (9)	57.4 (1)	Fe(1)–C(1)–Fe(2)	81.5 (9)	81.7 (9)
Fe(2)–Fe(1)–P(1)	53.4 (2)	53.0 (2)	Fe(1)–C(2)–O(2)	176 (3)	174 (3)
Fe(1)–Fe(2)–P(1)	53.0 (2)	53.6 (2)	Fe(1)–C(3)–O(3)	176 (2)	174 (3)
Ru–Fe(1)–P(1)	67.8 (2)	66.5 (2)	Fe(1)–C(4)–O(4)	172 (2)	172 (2)
Ru–Fe(2)–P(1)	67.4 (2)	66.5 (2)	Fe(2)–C(5)–O(5)	175 (2)	175 (2)
Fe(1)–Ru–N(1)	78.2 (5)	78.0 (5)	Fe(2)–C(6)–O(6)	173 (2)	176 (2)
Fe(2)–Ru–N(1)	77.4 (5)	78.2 (5)	Fe(2)–C(7)–O(7)	176 (3)	175 (2)
Fe(1)–P(1)–Fe(2)	73.6 (2)	73.3 (2)	Ru–C(8)–O(8)	179 (2)	175 (3)
Fe(1)–P(1)–N(1)	105.3 (6)	107.8 (7)	Ru–C(9)–O(9)	174 (2)	176 (2)
Fe(1)–P(1)–N(3)	130.2 (8)	123.5 (7)	Ru–C(10)–O(10)	174 (2)	176 (3)
Fe(2)–P(1)–N(1)	103.9 (6)	109.4 (7)	C(1)–Fe(1)–C(2)	175 (1)	173 (1)
Fe(2)–P(1)–N(3)	127.0 (8)	126.6 (7)	C(1)–Fe(1)–C(3)	82 (1)	83 (1)
Ru–N(1)–P(1)	93.3 (7)	89.4 (7)	C(1)–Fe(1)–C(4)	87 (1)	89 (1)
Ru–N(1)–P(2)	142 (1)	140 (1)	C(2)–Fe(1)–C(3)	93 (1)	92 (1)
Fe(2)–Fe(1)–C(1)	49.1 (7)	48.4 (7)	C(2)–Fe(1)–C(4)	96 (1)	96 (1)
Fe(1)–Fe(2)–C(1)	49.4 (7)	49.9 (7)	C(3)–Fe(1)–C(4)	102 (1)	99 (1)
Ru–Fe(1)–C(1)	97.4 (7)	96.3 (7)	C(1)–Fe(2)–C(5)	86 (1)	82 (1)
Ru–Fe(2)–C(1)	97.2 (7)	97.1 (8)	C(1)–Fe(2)–C(6)	175 (1)	176 (1)
P(1)–Fe(1)–C(1)	96.5 (7)	96.4 (7)	C(1)–Fe(2)–C(7)	86 (1)	86 (1)
P(1)–Fe(2)–C(1)	96.3 (7)	98.3 (7)	C(5)–Fe(2)–C(6)	90 (1)	94 (1)
Fe(2)–Fe(1)–C(2)	132.8 (8)	132.2 (8)	C(5)–Fe(2)–C(7)	103 (1)	102 (1)
Fe(2)–Fe(1)–C(3)	117.1 (7)	117 (1)	C(6)–Fe(2)–C(7)	98 (1)	93 (1)
Fe(2)–Fe(1)–C(4)	110.8 (8)	113.9 (8)	C(8)–Ru–C(9)	97 (1)	95 (1)
Ru–Fe(1)–C(2)	81.0 (1)	79.9 (9)	C(8)–Ru–C(10)	92 (1)	90 (1)
Ru–Fe(1)–C(3)	96.1 (8)	95 (1)	C(9)–Ru–C(10)	95 (1)	93 (1)
Ru–Fe(1)–C(4)	162.0 (8)	165.8 (8)	N(1)–P(1)–N(3)	110 (1)	110.8 (9)
P(1)–Fe(1)–C(2)	87.5 (8)	87.3 (9)	N(1)–P(2)–N(2)	116 (1)	115 (1)
P(1)–Fe(1)–C(3)	163.6 (8)	161 (1)	N(2)–P(3)–N(3)	117 (1)	121 (1)
P(1)–Fe(1)–C(4)	94.5 (8)	99.8 (9)	P(1)–N(1)–P(2)	125 (1)	130 (1)
Fe(1)–Fe(2)–C(5)	117.5 (7)	114.8 (8)	P(2)–N(2)–P(3)	122 (1)	120 (1)
Fe(1)–Fe(2)–C(6)	130.7 (7)	134.1 (8)	P(1)–N(3)–P(3)	128 (1)	118 (1)
Fe(1)–Fe(2)–C(7)	112 (1)	112.9 (7)	Cl(1)–P(2)–Cl(2)	102.2 (4)	100.5 (4)
Ru–Fe(2)–C(5)	91.8 (8)	91.6 (9)	Cl(3)–P(3)–Cl(4)	101.1 (5)	101.8 (5)
Ru–Fe(2)–C(6)	79.7 (8)	84.8 (8)	Cl(1)–P(2)–N(1)	108.8 (7)	112.1 (7)
Ru–Fe(2)–C(7)	164.8 (9)	166.5 (7)	Cl(1)–P(2)–N(2)	111.3 (8)	109.3 (8)
P(1)–Fe(2)–C(5)	159.1 (8)	158.0 (9)	Cl(2)–P(2)–N(1)	110.7 (7)	109.2 (8)
P(1)–Fe(2)–C(6)	86.2 (7)	86.1 (8)	Cl(2)–P(2)–N(2)	107.6 (8)	109.6 (8)
P(1)–Fe(2)–C(7)	98 (1)	100.1 (7)	Cl(3)–P(3)–N(2)	108.0 (8)	108.5 (8)
Fe(1)–Ru–C(8)	156.0 (7)	161.3 (8)	Cl(3)–P(3)–N(3)	111.1 (8)	109.4 (8)
Fe(1)–Ru–C(9)	107.1 (8)	102.9 (8)	Cl(4)–P(3)–N(2)	107.0 (8)	106.3 (8)
Fe(1)–Ru–C(10)	89.6 (8)	92 (1)	Cl(4)–P(3)–N(3)	111.0 (8)	107.6 (9)
Fe(2)–Ru–C(8)	98.6 (7)	104.0 (8)			
Fe(2)–Ru–C(9)	163.6 (9)	159.8 (8)	solvent		
Fe(2)–Ru–C(10)	90.6 (8)	93 (1)	C(O1)–C(O2)–C(O3)	123 (3)	
N(1)–Ru–C(8)	96.7 (8)	97.3 (9)	C(O3)–C(O2)–C(O3)[a]	114 (5)	
N(1)–Ru–C(9)	95.0 (9)	94.1 (9)	C(O2)–C(O3)–C(O4)	126 (4)	
N(1)–Ru–C(10)	166.1 (9)	169 (1)	C(O3)–C(O4)–C(O5)	119 (4)	
			C(O4)–C(O5)–C(O4)[a]	115 (6)	

[a] Symmetry related by $-x$, $-y$, z.

packed with hexane solvent. Elution with hexane brought about the separation of three bands: a green band containing $Fe_3(CO)_{12}$, a purple band containing **3** (0.13 g, 11%), and an orange fraction corresponding to unreacted **2** (0.85 g, 85%).

A similar reaction between **2** and $Fe(CO)_5$ (3-h reflux) yielded only trace quantities of **3** after chromatography of the reaction mixture. Some insoluble material was observed at the top of the silica column that did not elute with hexane or methylene chloride.

Reaction of $(NPCl_2)_3$ with $Na_2Fe(CO)_4 \cdot {}^3/_2$Dioxane. The reaction of equimolar amounts of $(NPCl_2)_3$ and $Na_2Fe(CO)_4$ was carried out in a similar manner to the reaction of $(NPCl_2)_3$ with $Na_2Fe_2(CO)_8$. After an identical isolation procedure, low yields of **2** (<2%) and **3** (trace) were obtained.

Synthesis of $N_3P_3Cl_4Fe_2Ru(CO)_{10}$ (7). $N_3P_3Cl_4Fe_2(CO)_8$ (**2**), (0.5 g, 0.8 mmol) and $Ru_3(CO)_{12}$ (1.3 g, 2.0 mmol) were placed in a 200-mL Schlenk flask, and heptane (100 mL) was added. The reaction mixture was stirred and heated at reflux for 3 h. The reaction mixture was then allowed to cool to room temperature. On cooling, some $Ru_3(CO)_{12}$ precipitated from solution. The solution was filtered, and the filtrate was poured directly onto a chromatography column packed with silica gel (coarse) as a hexane slurry. Chromatography resulted in the separation of three bands. Elution with hexane yielded an orange band that contained unreacted $Ru_3(CO)_{12}$ and the mixed-metal cluster $FeRu_2(CO)_{12}$. Use of a CH_2Cl_2 (10%)/hexane (90%) solvent mixture as the eluent removed a violet-red band, $N_3P_3Cl_4Fe_2Ru(CO)_{10}$ (**7**). Unreacted **2** was recovered by elution with 100% CH_2Cl_2. Removal of the solvent from the second fraction yielded a violet-red crystalline solid, **7** (0.032 g, 5% yield). Mass spectrum for **7**: m/e calcd 768.5285, found 768.5340. The yield of **7** was not improved by doubling the reaction time.

The separation of $Ru_3(CO)_{12}$ and $FeRu_2(CO)_{12}$ was achieved by column chromatography using a silica gel (fine) column and hexane as the eluent. $FeRu_2(CO)_{12}$ is a known compound,[44] and its identity was confirmed from infrared and mass spectral data. The infrared spectrum agreed with that reported[44] (ν_{CO} (cyclohexane) 2067 (s), 2042 (vs), 2034 (s), 2012 (w), 1988 (w) cm^{-1}). The electron-impact mass spectrum for $FeRu_2(CO)_{12}$ showed a parent peak at m/e 595, as well as ions corresponding to the loss of 12 carbonyl ligands.

Reactions of **2** with $Ru_3(CO)_{12}$ in refluxing hexane (similar to that described in the above section) for 4 h yielded only a trace of **7**. Increases in the reaction time to 12 h did not improve the yield of **7**. None of the mixed-metal cluster $FeRu_2(CO)_{12}$ was detected in these reactions.

X-ray Structure Determination. (a) Crystal Preparation. Crystals of each compound were grown from the solvents indicated in Table III. The general procedure used for growing suitable crystals was the following: The compound was dissolved in a minimum amount of solvent in a small flask and was placed in a Dewar insulator that contained a small quantity of water. This whole assembly was covered and placed in a freezer to ensure slow cooling of the solution. After crystal formation had occurred, a suitable crystal was mounted with epoxy cement on a glass fiber (approximately one-fourth the crystal diameter).

Table XII. Fractional Atomic Positional Parameters for 7

	A			B		
	x	*y*	*z*	*x*	*y*	*z*
Fe(1)	0.5561 (1)	0.3410 (1)	0.2614 (4)	0.9432 (1)	0.1575 (1)	−0.2972 (4)
Fe(2)	0.4780 (1)	0.2657 (1)	0.2444 (4)	1.0178 (1)	0.2367 (1)	−0.2938 (4)
Ru	0.54986 (7)	0.27716 (7)	0.0	0.95031 (7)	0.22351 (7)	−0.0399 (2)
Cl(1)	0.6097 (3)	0.1148 (2)	0.0169 (9)	0.8856 (2)	0.3870 (2)	−0.0765 (8)
Cl(2)	0.7083 (2)	0.1946 (3)	0.0550 (8)	0.7929 (3)	0.3001 (3)	−0.0505 (9)
Cl(3)	0.5765 (4)	0.1069 (3)	0.555 (1)	0.7834 (3)	0.2627 (3)	−0.572 (1)
Cl(4)	0.6780 (4)	0.1765 (4)	0.639 (1)	0.8534 (4)	0.3625 (4)	−0.675 (1)
P(1)	0.5646 (2)	0.2529 (2)	0.3131 (8)	0.9296 (2)	0.2461 (2)	−0.3475 (8)
P(2)	0.6374 (2)	0.1735 (2)	0.1564 (8)	0.8558 (2)	0.3213 (2)	−0.1904 (8)
P(3)	0.6213 (3)	0.1698 (3)	0.4748 (8)	0.8484 (3)	0.3069 (3)	−0.5064 (9)
N(1)	0.5940 (6)	0.2251 (7)	0.154 (2)	0.8977 (7)	0.2736 (7)	−0.196 (2)
N(2)	0.6517 (8)	0.1498 (8)	0.3230 (3)	0.8326 (8)	0.3402 (8)	−0.352 (2)
N(3)	0.5860 (8)	0.2233 (7)	0.463 (2)	0.9024 (7)	0.2695 (8)	−0.515 (3)
O(1)	0.4423 (7)	0.3790 (7)	0.344 (2)	1.0580 (8)	0.1263 (7)	−0.398 (2)
O(2)	0.6744 (7)	0.3412 (7)	0.184 (2)	0.8277 (8)	0.1541 (8)	−0.204 (3)
O(3)	0.5371 (8)	0.4489 (9)	0.112 (3)	0.9712 (9)	0.0553 (9)	−0.116 (3)
O(4)	0.5738 (9)	0.3827 (9)	0.576 (3)	0.9257 (9)	0.1165 (9)	−0.613 (3)
O(5)	0.3836 (7)	0.2928 (7)	0.039 (2)	1.1180 (8)	0.2164 (8)	−0.101 (2)
O(6)	0.4790 (7)	0.1499 (7)	0.145 (2)	1.0125 (7)	0.3544 (7)	−0.209 (2)
O(7)	0.4306 (8)	0.2430 (8)	0.552 (3)	1.0622 (8)	0.2580 (8)	−0.609 (3)
O(8)	0.5045 (7)	0.1849 (7)	−0.212 (2)	0.985 (1)	0.319 (1)	0.169 (3)
O(9)	0.6485 (8)	0.3101 (8)	−0.199 (3)	0.8521 (9)	0.1868 (8)	0.157 (3)
O(10)	0.4780 (9)	0.3631 (8)	−0.159 (3)	1.0285 (9)	0.1449 (9)	0.123 (3)
C(1)	0.474 (1)	0.346 (1)	0.304 (3)	1.025 (1)	0.157 (1)	−0.346 (3)
C(2)	0.626 (1)	0.341 (1)	0.210 (3)	0.875 (1)	0.155 (1)	−0.233 (3)
C(3)	0.5435 (9)	0.4050 (9)	0.167 (3)	0.960 (1)	0.095 (1)	−0.196 (4)
C(4)	0.566 (1)	0.362 (1)	0.454 (3)	0.931 (1)	0.129 (1)	−0.489 (4)
C(5)	0.4190 (9)	0.2805 (9)	0.121 (3)	1.079 (1)	0.222 (1)	−0.178 (4)
C(6)	0.4799 (9)	0.1962 (9)	0.174 (4)	1.016 (1)	0.308 (1)	−0.244 (3)
C(7)	0.447 (1)	0.253 (1)	0.430 (4)	1.0467 (9)	0.2497 (9)	−0.480 (3)
C(8)	0.5218 (9)	0.2204 (9)	−0.129 (3)	0.972 (1)	0.283 (1)	0.099 (3)
C(9)	0.611 (1)	0.295 (1)	−0.123 (3)	0.889 (1)	0.198 (1)	0.087 (3)
C(10)	0.5046 (9)	0.3288 (9)	−0.089 (3)	1.000 (1)	0.176 (1)	0.057 (4)
			Solvent			
C(O1)	0.0	0.5	0.700 (9)			
C(O2)	0.0	0.5	0.536 (7)			
C(O3)	−0.021 (2)	0.457 (2)	0.451 (5)			
C(O4)	−0.023 (2)	0.455 (2)	0.292 (6)			
C(O5)	0.0	0.5	0.201 (9)			

(b) Data Collection. A given crystal was optically centered on an Enraf-Nonius four-circle CAD4 automated diffractometer controlled by a PDP8/a computer coupled to a PDP11/34 computer. A full-rotation orientation photograph was taken with a Polaroid cassette accessory, and 25 intense reflections were chosen and centered with the use of manufacturer-supplied software.[50] The INDEX program was used to obtain an orientation matrix and unit cell parameters. Successive centerings and least-squares refinements of 2θ values found for the 25 precisely centered reflections gave the lattice constants listed in Table III for each of the crystals. Program TRACER was used to determine the appropriateness of the unit cell initially chosen, and a transformation was applied in cases where the initial choice was unsatisfactory. A small test data set (axial and zero layer reflections) was collected to determine the systematic absences, if any. The space groups thus chosen are listed in Table III and were confirmed by the successful refinement of the structures. The number of formula units per cell, Z (Table III), was determined on the basis of the measured density of each compound.

Intensity data were collected at room temperature (21 °C) with the use of a graphite single-crystal monochromator and Mo Kα radiation (λ = 0.71073 Å), take off angle 2.8°. A θ–2θ scan mode was used with 2θ ranging from $(A + 0.347 \tan \theta)°$ below the calculated position of Kα_1 reflection to $(A + 0.347 \tan \theta)°$ above the calculated position of the Kα_2 reflection. The A values are given in Table III. The scan rate was varied automatically from 1 to 5° min^{-1}, depending on the intensity of a reflection as determined by a preliminary brief scan. Background counts were measured with the detector stationary and positioned at the beginning and end of the scan, each for one-fourth of the total scan time. Three standard reflections were measured after periodic intervals of X-ray irradiation, and the same reflections were recentered automatically after every several hundred reflections to check on crystal orientation and stability. The total number of unique reflections observed for each compound are given in Table III, with the criterion for observation being $I > 2\sigma(I)$.

Linear absorption coefficients for MoKα radiation are also given in Table III (μ, cm^{-1}). The values were sufficiently small such that no absorption corrections were applied. The data were processed by manufacturer-supplied software.[50] The integrated intensity, I, was calculated according to the expression[51] $I = [SC - 2(B_1 + B_2)]T_r$, where SC is the count accumulated during the scan, B_1 and B_2 are the background counts at each end of the scan, and T_r is the 2θ scan rate in deg/min.

In all cases the standard reflections were used to rescale the data automatically to correct for drift due to changes in temperature, centering, etc. during data collection. The ranges of random long-term drift are indicated in Table III. The unique, normalized, integrated intensity set was processed to give F and E values. The polarization corrections were calculated on the assumption that the incident beam is polarized to some extent by the monochromator. The graphite crystal was assumed to be 50% perfect and 50% perfectly mosaic for this purpose.

Structure Solution and Refinement. The positions of the metal atoms in each case were established from a sharpened, origin-removed Patterson map and were confirmed by a direct methods solution. The remaining non-hydrogen atoms were located with one or two Fourier syntheses. Hydrogen atoms for compound **3** were located at their calculated positions. In the case of methyl groups, a tetrahedral model was used wherein the hydrogen atoms were placed at positions giving the closest agreement with the peaks found in the difference Fourier maps (C–H = 0.97 Å). All hydrogen atoms were assigned fixed isotropic temperature parameters[52] of B = 5.0 Å^2. None of the parameters for the hydrogen atoms was varied. All non-hydrogen atoms were refined anisotropically for compound **2**. For compounds **3** and **7**, the carbonyl groups and the toluene molecule were refined only isotropically. Neutral-atom scattering

(50) All programs used in data collection, reduction, and refinement are part of the: "Enraf-Nonius Structure Determination Package"; Enraf-Nonius: Delft, The Netherlands, 1975, revised 1977.

(51) Corfield, P. W. R.; Doedens, R. J.; Ibers, J. A. *Inorg. Chem.* **1967**, *6*, 197.

(52) Isotropic thermal parameters are of the form $\exp[-B(\sin^2 \theta)/\lambda^2]$.

factors were those given by Cromer and Mann[53] and by Stewart et al.[54] for non-hydrogen and hydrogen atoms, respectively. Real and imaginary anomalous dispersion corrections to the atomic scattering factors were included.[55] In the last cycle of least-squares refinement the maximum parameter shift was less than 0.32 of a standard deviation. The final R values[56] are listed in Table III. Final difference Fourier maps showed the residual electron density (e Å^3) for each structure as indicated in Table III.

(53) Cromer, D. T.; Mann, J. B. *Acta Crystallogr., Sect. A* **1968**, *A24*, 321.
(54) Stewart, R. F.; Davidson, E. R.; Simpson, W. T. *J. Chem. Phys.* **1965**, *42*, 3175.
(55) "International Tables for X-Ray Crystallography", 3rd ed.; Kynoch Press: Birmingham, United Kingdom, 1968; Vol. III, Table 3.3.2C, pp 2115–2116.
(56) $R_1 = \sum||F_o| - |F_c||/\sum|F_o|$; $R_2 = [\sum w(|F_o| - |F_c|)^2/\sum w(F_o)^2]^{1/2}$, $w = 1/\sigma(F_o)^2$.

Acknowledgment. We thank the U.S. Army Research Office for the support of this work through Grant No. DAAG 2982-K-0045, and G. L. Lang for the Mössbauer data. The Mössbauer work was supported by the National Institutes of Health through Grant No. HL-16860. We also thank R. A. Nissan and J. L. Desorcie for obtaining the NMR data.

Registry No. 1, 940-71-6; **2**, 83437-98-3; **3**, 83447-76-1; **4**, 2950-45-0; **5**, 90866-55-0; **6**, 90866-56-1; **7**, 90866-57-2; $Na_2Fe_2(CO)_8$, 64913-30-0; $Na_2Fe(CO)_4$, 14878-31-0; $Fe(CO)_5$, 13463-40-6; $Fe_2(CO)_9$, 15321-51-4; $Ru_3(CO)_{12}$, 15243-33-1; Fe, 7439-89-6; Ru, 7440-18-8.

Supplementary Material Available: Listing of thermal parameters, root mean square displacements, and observed and calculated structure factors for compounds **2**, **3**, and **7** (51 pages). Ordering information is given on any current masthead page.

Host–Guest Complexation. 30. Quinquaryl and Bis(urea) Binders[1]

Howard E. Katz and Donald J. Cram*

Contribution from the Department of Chemistry of the University of California at Los Angeles, Los Angeles, California 90024. *Received January 10, 1984*

Abstract: Six new types of macrocycles and one open-chain analogue are described, along with their conformational behavior and binding free energies toward alkali metal, ammonium, and alkylammonium picrates. The cycles are 20-membered and are composed by attaching aryloxy, cyclic urea, pyridyl, ethylene, methylene, and oxygen units to one another. The structures and points of attachment of all but the latter two units are drawn and are symbolized by capital letters. The structures of

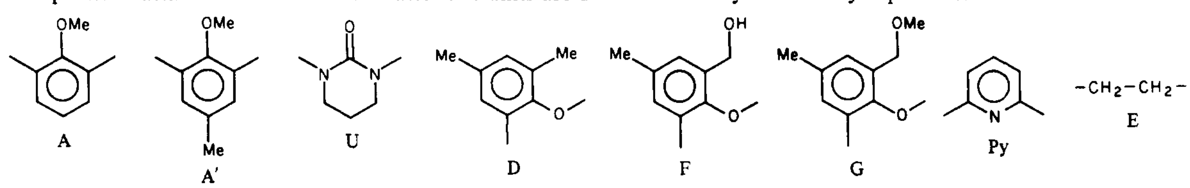

the hosts and the synthetic intermediates are indicated by line formulas consisting of sequences of letters which represent the sequences of units bonded to one another in the hosts. The key intermediate in the synthesis of A′(A′DE)$_2$O (**5**) and A′(A′DCH$_2$)$_2$Py (**6**) was bis(phenol) A′(A′DH)$_2$ (**18**). Ring closure of this compound with $O(CH_2CH_2OTs)_2$ and base gave A′(A′DE)$_2$O (**5**, 49%) and with $BrCH_2PyCH_2Br$ and base gave A′(A′OCH$_2$)$_2$Py (**6**, 11%). Treatment of the second key intermediate, bis(phenol) A(UDH)$_2$ (**32**), with $O(CH_2CH_2OTs)_2$ and base gave A(UDE)$_2$O (**7**, 56%) and with $BrCH_2PyCH_2Br$ and base gave A(UDCH$_2$)$_2$Py (**8**, 29%). A mixture of the third key intermediate, bis(hydroxymethylphenol) A(UFH)$_2$ (**33**), with $BrCH_2PyCH_2Br$ and base gave bis(hydroxymethylene) compound A(UFCH$_2$)$_2$Py (**9**, 47%), methylation of which produced A(UGCH$_2$)$_2$Py (**10**, 82%). Methylation of A(UFH)$_2$ (**33**) directly gave open-chain reference compound A(UFMe)$_2$ (**11**, 38%). Spectral experiments (^{1}H NMR and ^{13}C NMR) demonstrated that free cycles A(UDCH$_2$)$_2$Py (**8**), A(UFCH$_2$)$_2$Py (**9**), and A(UGCH$_2$)$_2$Py (**10**) exist in solution as two conformers, one that binds guests (binding or B′ conformer) and one that is nonbinding (N′ conformer). In solution, the two conformers equilibrate observably on the human and slowly on the ^{1}H NMR time scales. When treated with guest, each host gives a single complex formed instantaneously with B′ but over a period of hours with N′. Interestingly, A(UDCH$_2$)$_2$Py (**8**) crystallizes in the free state and as its $NaClO_4$ complex as its binding (B′) conformer, which is disfavored in $CDCl_3$ solution at equilibrium ([N′]/[B′] = 3 at 28 °C). In the absence of polar or ionic catalysts, the B′ conformer goes to the N′ conformer at 28 °C with $\Delta G^* \sim 22$ kcal mol^{-1}. In contrast, A(UFCH$_2$)$_2$Py (**9**) crystallizes as its nonbinding (N′) conformer, which also predominates in the free state in $CDCl_3$–$DCON(CD_3)_2$ solution ([N′]/[B′] = 2.2 at 28 °C). Molecular models and NMR spectral comparisons suggest that the N′ conformations of A(UDCH$_2$)$_2$Py (**8**), A(UFCH$_2$)$_2$Py (**9**), and A(UGCH$_2$)$_2$Py (**10**) either have their single methyl groups or their two methylene groups turned inward to fill their cavities. The binding free energies ($-\Delta G°$) at 25 °C in $CDCl_3$ saturated with D_2O were determined by the extraction technique for hosts **5**–**11** binding the picrate salts of Li^+, Na^+, K^+, Rb^+, Cs^+, NH_4^+, $CH_3NH_3^+$, and t-$BuNH_3^+$. Maximum binding by the six cycles of the guests was observed for Na^+ or K^+ ions, with $-\Delta G°$ values in the 13.3–10.0 kcal mol^{-1} range. Quinquaryl systems, A′(A′DE)$_2$O (**5**) and A′(A′DCH$_2$)$_2$Py (**6**), were stronger binders of all ions (except t-$BuNH_3^+$) than the cyclic urea-containing hosts **7**–**10**, a fact attributed to the higher degree of preorganization for binding of the former compounds. All cycles showed high values for complexing $CH_3NH_3^+$, which ranged from 11.3 kcal mol^{-1} for A′(A′DCH$_2$)$_2$Py (**6**) to 9.0 kcal mol^{-1} for A′(A′DE)$_2$O (**5**) and A(UDCH$_2$)$_2$Py (**8**). The highest structural recognition of host toward guest was observed with A′(A′DCH$_2$)$_2$Py (**6**) binding $CH_3NH_3^+$ 5.3 kcal mol^{-1} better than t-$BuNH_3^+$ (factor of 8000 difference in association constants). The same host favored binding Na^+ over Li^+ by 4.7 kcal mol^{-1} (factor of 3000). Of the six cyclic hosts, this one showed the highest binding and greatest discrimination among ions. Molecular model comparisons of **5**–**11** show A′(A′DCH$_2$)$_2$Py (**6**) to be the most rigidly preorganized for binding. The structure and discrimination in binding of this system nicely illustrate the principles of complementarity and preorganization in complexation. Flexible open-chain model host A(UFCH$_3$)$_2$ (**11**) showed peak binding for Cs^+ at $-\Delta G° = 6.5$ kcal mol^{-1}. It also bound ions K^+ and larger with values that ranged from 5.8 to 6.2 kcal mol^{-1}. The terminal hydroxyl groups probably hydrogen bond one another in its complexes.

Earlier papers demonstrated that appropriate combinations of p-methylanisyl, cyclic urea, methylene, methyleneoxy, and ethyleneoxy units to form 18-membered to 21-membered ring macrocycles resulted in hosts that were both stronger and more

